SIAM J. Applied Dynamical Systems
Vol. 3, No. 3, pp. 191–231

Pattern Formation in a Network of Excitatory and Inhibitory Cells with Adaptation*

Rodica Curtu† and Bard Ermentrout†

Abstract. A bifurcation analysis of a simplified model for excitatory and inhibitory dynamics is presented. Excitatory cells are endowed with a slow negative feedback and inhibitory cells are assumed to act instantly. This results in a generalization of the Hansel–Sompolinsky model for orientation selectivity. Normal forms are computed for the Turing–Hopf instability, where a new class of solutions is found. The transition from stationary patterns to traveling waves is analyzed by deriving the normal form for a Takens–Bogdanov bifurcation. Comparisons between the normal forms and numerical solutions of the full model are presented.

Key words. pattern formation, neural networks, normal forms, Takens–Bogdanov

AMS subject classifications. 34C15, 34C23, 34C25, 37G15, 37N25, 92C20

DOI. 10.1137/030600503

1. Introduction.

Many areas of the brain have a sheet-like architecture in which neurons interact horizontally through some spatial distribution. This is useful since it provides a substrate for topographic connectivity in sensory areas such as vision and touch. For example, in vision, nearby areas in the retina project to nearby areas in the visual cortex [16]. Spatial coding is not the only organizing principle in cortical networks. Neurons that respond preferentially to similar stimuli are more strongly linked than those responding to different stimuli. A classic example of this is orientation preference in the visual cortex [15]. Neurons in parts of the visual cortex respond to oriented bars of light and many of these cells have a preferred angle. Thus, topologically, we can regard the network as lying on a ring of length π corresponding to all possible orientations. Similar organizing principles based on angular preference are also seen in the head-direction system of rodents [25]. Experiments in which slices are removed from the cortex and pharmacologically manipulated (to make them more excited) support propagating waves [2]. This shows that the "wiring" between neurons is spatially organized.

In the simplest sense, cortical neurons can be divided into excitatory and inhibitory cells. Most excitatory, or regular-spiking, neurons have some form of spike-frequency adaptation (SFA). That is, there is a slow intrinsic negative feedback term which lowers the firing rate of the neuron when a constant current is applied. In contrast, inhibitory, or fast-spiking, neurons generally do not have a similar rate adaptation. In the classic models of Wilson and Cowan [24], excitatory and inhibitory cells are treated the same with a single scalar number (the firing rate) associated with each neuron. In a recent model for feature selectivity, Hansel

*Received by the editors July 18, 2003; accepted for publication (in revised form) by M. Golubitsky February 4, 2004; published electronically July 6, 2004. This work was supported in part by the National Science Foundation.
http://www.siam.org/journals/siads/3-3/60050.html
†Department of Mathematics, University of Pittsburgh, Pittsburgh, PA 15260 (rodicacurtu@unitbv.ro, bard@pitt.edu).

and Sompolinsky [15] introduce a rate model in which the excitatory cells are endowed with SFA. The domain of their model is a circle corresponding to orientation preference. Because the model is piecewise-linear they are able to analyze a number of interesting patterns. The motivation for the model is to shed light on the importance of recurrent (nonlinear feedback) connections in setting the orientation selectivity to broadly tuned inputs. (That is, they present an input with a small local maximum in orientation and ask if the network can amplify the difference between the peak and the background.) They find that, even in the absence of input, their network is able to support local peaks of activity; the inputs serve to position the peak by breaking the rotational symmetry of the model. Interestingly, they show that the presence of SFA causes the local peak to rotate around the circle in the form of a traveling wave. They exploit the piecewise linear nature of their model to determine parameter regimes where traveling waves exist as a function of the adaptation.

Our goal in this paper is to generalize the nonlinearity used in their model and then use methods from dynamical systems to study and characterize the nonlinear behavior. We first state the model equations and simplify it so that it becomes a two-variable model (neural firing rate and degree of adaptation). The spatial interactions are of the lateral-inhibition type; there is local excitation of nearby spatial points (or features) and inhibition at distant points. With weak or rapidly decaying adaptation, we show that there is a bifurcation to stationary spatial patterns. These correspond to the peaked patterns computed in the Hansel–Sompolinsky (HS) model. Moreover, with strong or slowly decaying adaptation, there is a Hopf bifurcation to spatially varying patterns. Under some circumstances, these correspond to the traveling waves in the HS model; however, depending on the nonlinearity, there are also standing oscillations. Finally, we look at the point of transition between stationary and oscillating patterns. This occurs at a Takens–Bogdanov bifurcation and leads to some interesting and complex behavior. This latter part occupies the bulk of the paper.

While normal forms have been computed generally for systems undergoing a Hopf bifurcation or Takens–Bogdanov bifurcation in the presence of $O(2)$ symmetry, there are many qualitatively different normal forms. Thus, in order to apply these methods to a specific problem, it is necessary to actually compute the coefficients. Thus, we describe the highlights of the calculation in the main text and leave the details to Appendix A. One of the main reasons for computing the coefficients is so that we can find regions in parameter space, where new types of behavior occur. In particular, we have found conditions on the nonlinearity such that standing waves occur. These are not found in the original HS model, where the nonlinearity was piecewise-linear.

1.1. HS model. Hansel and Sompolinsky [15] introduced a simple rate-model for the study of feature selectivity in local cortical circuits. In that context the network of neurons was assumed to code for a sensory or movement scalar feature x (for example, the angle a bar is rotated in the subject receptor field so that x can be taken in the interval $[-\frac{\pi}{2}, \frac{\pi}{2}]$). The local cortical network consists of ensembles of neurons that respond (are tuned) to a particular feature of an external stimulus, and so are called "feature columns," and that are interconnected by recurrent synaptic connections. In other words, each neuron in the network is selective, firing maximally when a feature ("preferred feature" of the neuron) with a particular value is present. The synaptic interactions between a presynaptic neuron y from the β-population and a postsynaptic neuron x from the α-population are denoted by a function

$J^{\alpha\beta}(x-y) = j_0^{\alpha\beta} + j_2^{\alpha\beta}\cos(2(x-y))$, where α and β indices stand for E (excitatory) and/or I (inhibitory) populations of neurons, depending on the context. We take $j_0^{\alpha E} \geq j_2^{\alpha E} \geq 0$ for input coming from the excitatory population and $j_0^{\alpha I} \leq j_2^{\alpha I} \leq 0$ for input coming from the inhibitory population.

Hansel and Sompolinsky collapsed both excitatory and inhibitory populations into a single equivalent population. In this case the synaptic connectivity function J is defined as $J(x-y) = j_0 + j_2\cos(2(x-y))$ with no restrictions on the sign of coefficients, and the rate-model has a single rate variable $m(x,t)$ that represents the activity of the population of neurons in the column x at time t. Moreover, the population is assumed to display adaptation. The resulting model [15] is

$$\begin{aligned} \tau_0 \frac{\partial m}{\partial t}(x,t) &= -m(x,t) + F\left(\frac{1}{\pi}\int_{-\frac{\pi}{2}}^{\frac{\pi}{2}} J(x-y)m(y,t)dy + I^0(x-x_0) - I_a(x,t) - T\right), \\ \tau_a \frac{\partial I_a}{\partial t}(x,t) &= -I_a(x,t) + J_a\, m(x,t)\,. \end{aligned} \tag{1.1}$$

I^0 stands for the synaptic currents from the external neurons, T is the neuronal threshold, I_a is the adaptation current, $\tau_a > \tau_0$ is its time constant, and J_a measures the strength of adaptation.

An additional assumption for (1.1) is that the stable state of the network is such that all the neurons are far from their saturation level, allowing the gain function F to be in a semilinear form $F(I) = I$ for $I > 0$, and zero otherwise.

The model we analyze in this paper is based on the above HS model but includes a more general nonlinear gain function F. It also can be used in a more general context of synaptically coupled populations of excitatory and inhibitory neurons with adaptation.

1.1.1. A more general class of models. More generally, the problem we are interested in concerns the possible patterns that can be obtained in a neuronal network consisting of both excitatory and inhibitory cells, and in the presence of adaptation. The network model consists of two homogeneous populations of neurons, one excitatory (E), displaying adaptation, and the other one inhibitory (I), without adaptation. This is a reasonable assumption, for example, for *cortical neurons*, since experimental studies report that in the cortex most of the inhibitory neurons do not display spike adaptation [3], [4], [14].

The spatial connectivity is assumed to be all-to-all from E to E, E to I, and I to E cells, and in all cases the strength of the interactions decreases with the distance between neurons according to a Gaussian distribution with zero mean, say J_{EE}, J_{IE}, and J_{EI}, respectively. For simplicity, no I to I interactions are included. In addition, the network is considered one-dimensional in space.

We assume in the following a *linear adaptation* and describe the neuronal activity by a rate-model. That is, we have

$$\begin{aligned} \tau_E \frac{du_E}{dt} &= -u_E + F_E(J_{EE} * u_E - J_{EI} * u_I - gA)\,, \\ \tau_I \frac{du_I}{dt} &= -u_I + F_I(J_{IE} * u_E)\,, \\ \tau_A \frac{dA}{dt} &= -A + u_E\,, \end{aligned} \tag{1.2}$$

where τ_E, τ_I, τ_A are the time constants for the excitatory and inhibitory neurons, and for adaptation, respectively; A is the variable that defines the adaptation; g is the strength of adaptation; F_E and F_I are the firing-rate functions; and $J_{ij} * u_j$, with $i, j \in \{E, I\}$, is the convolution $J_{ij} * u_j(x,t) = \int_{-\infty}^{\infty} J_{ij}(x-y)u_j(y,t)\,dy$. Pinto and Ermentrout [20] analyzed a model like this, without the inhibitory interactions, in order to study propagating waves.

One simplification is to assume that the inhibition is much faster than the excitation, and that the firing rate for the inhibitory population is linear. That allows us to replace the equation for I cells with its steady state, i.e., to take $u_I \approx F_I(J_{IE} * u_E) = J_{IE} * u_E$. Then, since a convolution of two Gaussians with zero mean is still a Gaussian with zero mean, we have $(J_{EE} * u_E - J_{EI} * u_I)(x,t) = (\, J_{EE} - J_{EI} * J_{IE}\,) * u_E(x,t) = J * u_E(x,t)$, where $J(x)$ is a difference of two Gaussians. Therefore system (1.2) can be reduced to a rate-model for only one variable u, in which we include the neuronal activity for both excitatory and inhibitory populations, and with the synaptic coupling defined by a function J as in Figure 1(a) (the "Mexican hat").

In [10] one of us showed the existence of traveling waves in a two-population model without adaptation. In this work, in order to get a Hopf bifurcation at a nonzero wavenumber, it was necessary to assume that the inhibition was slow and that the range of inhibitory-inhibitory interactions exceeded that of the excitatory-excitatory interactions. This is not a realistic assumption for the sensory cortex, where the inhibition is more localized and acts rapidly. In this older work, excitatory cells were treated the same as inhibitory cells. However, it is now known that excitatory cells exhibit pronounced adaptation; thus we have included this in the model. Below, we describe conditions under which both Hopf and Takens–Bogdanov bifurcations occur in the more general problem, where the inhibitory cells are treated as a separate population.

1.1.2. Mathematical model. Under the assumptions considered in the previous section, the mathematical model equivalent to (1.2) is

$$\begin{aligned} \frac{\partial u}{\partial t} &= -u(x,t) + F\left(\alpha\, J * u\,(x,t) - g\, v(x,t)\right), \\ \tau\,\frac{\partial v}{\partial t} &= -v(x,t) + u(x,t) \end{aligned} \tag{1.3}$$

with $x \in \mathbb{R}$ the one-dimensional spatial coordinate, and α, g, and τ positive parameters.

The variables u and v represent the neuronal activity and adaptation, respectively, τ and g correspond to the time constant and the strength of adaptation, and α is a parameter that controls the strength of the synaptic coupling J.

Synaptic coupling. J is a continuous and even function, $J(-x) = J(x)\ \forall x \in \mathbb{R}$, and is absolutely integrable on the interval $[-l, l]$, where $l \in \mathbb{R}_+ \cup \{\infty\}$. If $l = \infty$, we ask that $\lim_{x\to-\infty} J(x) = \lim_{x\to\infty} J(x) = 0$. Otherwise, J is assumed to be periodic of period $2l$. Then the operator $J * u$ is defined as

$$J * u\,(x,t) = \int_{-l}^{l} J(x-y)\,u(y,t)\,dy\,. \tag{1.4}$$

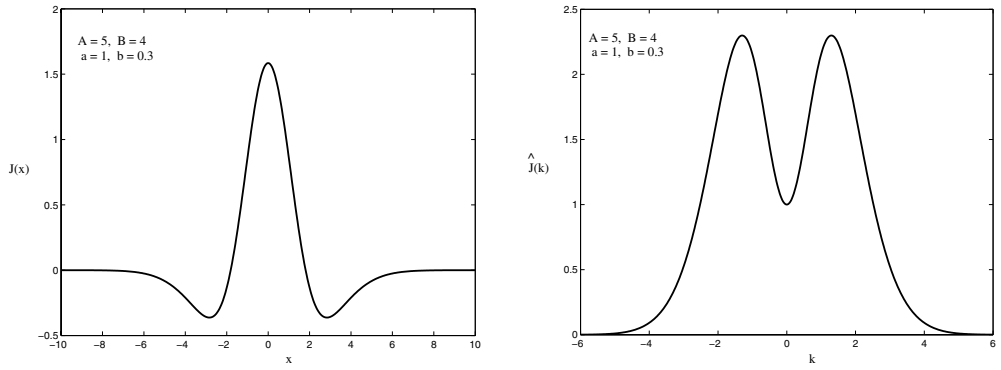

Figure 1. (a) *The coupling* $J(x) = \frac{1}{\sqrt{\pi}}\left[A\sqrt{a}\,e^{-ax^2} - B\sqrt{b}\,e^{-bx^2}\right]$ *for* $A = 5$, $B = 4$, $a = 1$, $b = 0.3$. (b) *The function* $\hat{J}$.

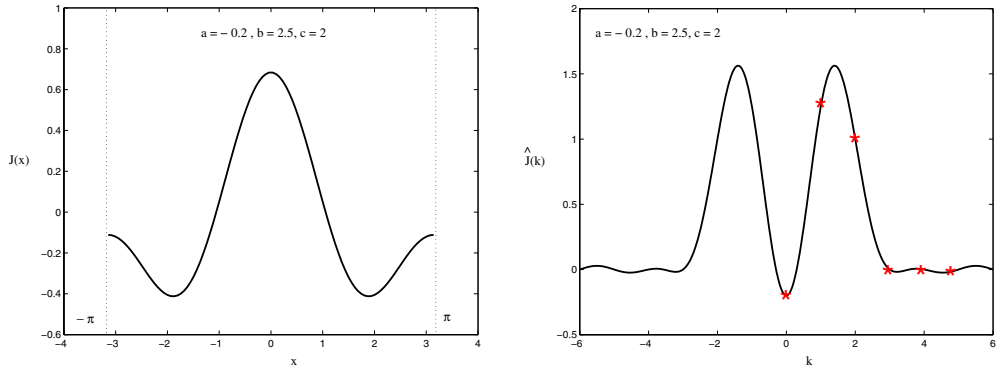

Figure 2. (a) *The periodic coupling* $J(x) = \frac{1}{2l}\left[a + b\cos(\frac{\pi x}{l}) + c\cos(\frac{2\pi x}{l})\right]$ *for* $l = \pi$ *and* $a = -0.2$, $b = 2.5$, $c = 2$. (b) *The function* $\hat{J}$.

There is an operator associated to J, which is defined on the frequency space, and that is

$$\hat{J}(k) = \int_{-l}^{l} J(x)\, e^{ikx}\, dx\,. \tag{1.5}$$

Remark 1. If we consider an infinite neural network, we take $l = \infty$ and the function J is typically as in Figure 1(a). For example, we can define J as

$$J(x) = \frac{1}{\sqrt{\pi}}\left[A\sqrt{a}\,e^{-ax^2} - B\sqrt{b}\,e^{-bx^2}\right],\ x \in \mathbb{R}\,, \tag{1.6}$$

where $A \geq B > 0$, $a > b > 0$. Then $\hat{J}(k) = A\,e^{-k^2/4a} - B\,e^{-k^2/4b}$, $k \in \mathbb{R}$, and $\hat{J}$ has the graph as in Figure 1(b). Nevertheless, in numerical simulations we cannot consider an infinite domain. Therefore we have to restrict ourselves to a finite domain $[-l, l]$ with $l \in \mathbb{R}_+$ and work with periodic boundary conditions. In order to maintain the assumptions of local excitation and long range inhibition, J is typically as in Figure 2(a). For example, we can take J as

$$J(x) = \frac{1}{2l}\left[a + b\,\cos\left(\frac{\pi x}{l}\right) + c\,\cos\left(\frac{2\pi x}{l}\right)\right],\ x \in \mathbb{R}\,, \tag{1.7}$$

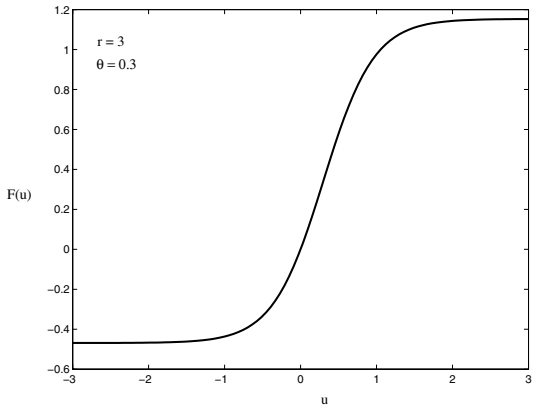

Figure 3. *The firing rate* (1.8) *for* $r = 3$ *and* $\theta = 0.3$.

where a, b, c are real parameters. Therefore $\hat{J}$ (see Figure 2(b)) is

$$\hat{J}(0) = a\,,\ \hat{J}(\pm\pi/l) = b/2\,,\ \hat{J}(\pm 2\pi/l) = c/2\,,\ \hat{J}(\pm j\pi/l) = 0\ \ (j \in \mathbb{N}\setminus\{0,1,2\})\,,$$
$$\hat{J}(k) = \frac{\sin(lk)\,[(a-b+c)(lk/\pi)^4 + (-5a+4b-c)(lk/\pi)^2 + 4a]}{lk\,[\,(lk/\pi)^2 - 1\,][\,(lk/\pi)^2 - 4\,]}\,,\ k \notin \pm(\pi/l)\mathbb{N}\,.$$

Firing rate. F in (1.3) is a sigmoid function (Figure 3) assumed to satisfy

$$F(0) = 0\,,\ F'(0) = 1\,.$$

The first condition translates the steady state to the origin $\bar{u} = 0$, $\bar{v} = 0$. The second condition brings additional simplifications to our calculations. A typical expression for F is then $F(u) = K\big[\frac{1}{1+e^{-r(u-\theta)}} - \frac{1}{1+e^{r\theta}}\big]$, with r and θ positive parameters, and $K = (1+e^{r\theta})^2\,e^{-r\theta}/r$, i.e.,

$$F(u) = \frac{1+e^{r\theta}}{r}\cdot\frac{1-e^{-ru}}{1+e^{-r(u-\theta)}}\,. \tag{1.8}$$

Remark 2. The condition $F'(0) = 1$ is not essential. As long as $F'(0)$ is nonzero and positive, the results proved in the following sections remain valid. To see this, let us assume that $F'(0) \neq 1$. Then, by the change of variables $u_{\text{new}} = u/F'(0)$, $v_{\text{new}} = v/F'(0)$, the change of parameters $\alpha_{\text{new}} = F'(0)\,\alpha$, $g_{\text{new}} = F'(0)\,g$, and the change of function $F_{\text{new}} = F/F'(0)$, we obtain a system topologically equivalent to (1.3), where F_{new} satisfies the constraints $F_{\text{new}}(0) = 0$ and $F'_{\text{new}}(0) = 1$.

Remark 3. The shape of F is also not crucial since we need only local properties of F, such as its first few derivatives. Thus, all we need for the analysis is that F have continuous third derivatives at the origin. However, most neural models use some sort of sigmoidal nonlinearity. The piecewise-linear model is dangerous since solutions can grow without bound under some circumstances.

2. Linear stability analysis and pattern initiation mechanism. Previous studies on reaction diffusion pattern generation mechanisms (see [19] for a review) and neural models of

pattern generation (such as a mechanism for stripe formation in the visual cortex [22], a model for the brain mechanism underlying visual hallucination patterns [10], [12], or a neural activity model for shell patterns [11]) indicate that in one-dimensional structures the linear theory turns out to be a good predictor of the ultimate steady state of the full nonlinear system. There is very good agreement between the theoretical solutions obtained from the linearized problem, and the numerical simulations of the original nonlinear system with initial conditions taken to be small random perturbations about the steady state.

Nevertheless, in order to find the solution of the linearized problem that corresponds to the stable spatial or spatio-temporal pattern that appears when the zero steady state loses stability, nonlinear terms of the original system must be taken into account, and a singular perturbation analysis around a bifurcation point must be pursued.

In the following we investigate the possible spatial and spatio-temporal patterns that can occur in the neuronal system with adaptation (1.3), as we vary the parameters α, g, τ, and θ.

Based on the hypotheses $F(0) = 0$, $F'(0) = 1$, the expansion of (1.3) in linear and higher order terms becomes

$$\begin{aligned} \frac{\partial u}{\partial t} &= -u + (\alpha J * u - gv) + \frac{F''(0)}{2}(\alpha J * u - gv)^2 + \frac{F'''(0)}{6}(\alpha J * u - gv)^3 + \cdots , \\ \frac{\partial v}{\partial t} &= (-v + u)/\tau , \end{aligned} \tag{2.1}$$

and then the linear operator is

$$L_0 U = \frac{\partial}{\partial t} U - \begin{pmatrix} -1 + \alpha J * (\cdot) & -g \\ 1/\tau & -1/\tau \end{pmatrix} U , \tag{2.2}$$

where $U = (u, v)^T$. We look for solutions of $L_0 U = \mathbf{0}$ that are bounded and have the form $\xi(t)\, e^{ikx}$ with $k \in \mathbb{R}$.

Let us assume first that $l = \infty$. Then, according to (1.4) and (1.5), equation (2.2) can be written as $\left[\frac{d\xi}{dt} - \hat{L}(k)\xi(t)\right] e^{ikx} = \mathbf{0}$, where

$$\hat{L}(k) = \begin{pmatrix} -1 + \alpha \hat{J}(k) & -g \\ 1/\tau & -1/\tau \end{pmatrix} . \tag{2.3}$$

Since we work on an infinite domain ($l = \infty$) and J is symmetric, this statement is true for all values of $k \in \mathbb{R}$. Moreover, we have $\hat{J}(-k) = \hat{J}(k)$.

The equation to be solved now is the ODE $\frac{d\xi}{dt} = \hat{L}(k)\xi$, which has two independent solutions $\xi_{1k}\, e^{\lambda_{1k} t}, \xi_{2k}\, e^{\lambda_{2k} t}$, where $\xi_{1,2\,k}$ are two-dimensional complex vectors. Therefore the eigenfunctions of L_0 have the form $\xi_{1,2\,k}\, e^{\lambda_{1,2\,k} t \pm ikx}$ and $\overline{\xi}_{1,2\,k}\, e^{\overline{\lambda}_{1,2\,k} t \mp ikx}$, where $\lambda_{1,2\,k}$ are the eigenvalues defined by

$$\lambda_{1,2\,k} = \frac{1}{2}\left[Tr(\hat{L}(k)) \pm \sqrt{Tr(\hat{L}(k))^2 - 4 \det(\hat{L}(k))} \right] .$$

If $\det(\hat{L}(k)) > 0$ and $Tr(\hat{L}(k)) < 0$ for all k, i.e., $\alpha\, \hat{J}(k) < g + 1$ and $\alpha\, \hat{J}(k) < 1/\tau + 1$, then all eigenfunctions of L_0 lie on the stable manifold and decay exponentially in time to zero. The trivial solution is asymptotically stable.

Remark 4. The eigenvalues k represent a measure of the wave-like pattern that can occur in the system. That is why k are called *wavenumbers*, or *modes*, of the system, and $2\pi/k$ are called *wavelengths*.

We consider k_0 to be *the most unstable mode*, defined as

$$\hat{J}(k_0) = \max_{k\geq 0}\hat{J}(k) = \max_{k\geq 0}\left(\int_{-\infty}^{\infty} J(x)\, e^{ikx}\, dx\right), \tag{2.4}$$

and assume that

$$k_0 \neq 0 \quad \text{and} \quad \hat{J}(k_0) > 0\,, \tag{2.5}$$

$$\hat{J}(k_0) \neq \hat{J}(k)\ \forall k \neq \pm k_0\,. \tag{2.6}$$

This is true for functions J as in Figure 1.

There are only two ways the trivial solution can lose its stability: either when the determinant becomes zero or when the trace becomes zero. We notice that (2.4), with additional conditions (2.5), (2.6), implies that $Tr(\hat{L}(k)) < Tr(\hat{L}(k_0))$ and $\det(\hat{L}(k)) > \det(\hat{L}(k_0))$ for $k \neq \pm k_0$. Therefore k_0 is the first eigenvalue in which the system may lose its stability; that is, k_0 is the most unstable mode of system (1.3). For all $k \neq \pm k_0$ the eigenfunctions belong to the stable manifold. On the other hand, the eigenfunctions with $\pm k_0$ wavenumber may form a basis for the center manifold that becomes our point of interest.

The wavenumber k_0 determines then the mechanism that generates the emerged pattern. There are basically two possible cases. At $\alpha\,\hat{J}(k_0) = g+1$, $g < 1/\tau$, the determinant becomes zero and a spatial pattern (steady state (SS)) bifurcates. At $\alpha\,\hat{J}(k_0) = 1 + 1/\tau$, $g > 1/\tau$, the trace becomes zero and a spatio-temporal pattern (traveling wave (TW)/standing wave (SW)) bifurcates.

Let us assume now that l is finite. There is a considerable difference between working with finite domains as the interval $[-l, l]$ and periodic boundary conditions. The difference comes from the fact that in this case there is only a discrete set of possible wavenumbers. The wavenumbers k must satisfy the condition $k \in \left(\pm\frac{\pi}{l}\mathbb{N}\right)$ in order for the integral $\int_{-l}^{l} J(x-y)\, e^{ik(x-y)}\, dy$ to be independent of x and so equal to $\hat{J}(k) = \int_{-l}^{l} J(y)\, e^{iky}\, dy$.

This allows us to use the matrix $\hat{L}(k)$ from (2.3) and construct the eigenvalues and eigenfunctions of the linear operator, as in the case of infinite domain. Moreover, the discussion from the previous paragraph remains valid here with the observation that in the case of l finite we consider *only* those values of k belonging to the set $\left(\pm\frac{\pi}{l}\mathbb{N}\right)$.

The most unstable mode k_0 is then defined as

$$\hat{J}(k_0) = \hat{J}\left(\frac{\pi n_0}{l}\right) = \max_{k\in\frac{\pi\mathbb{N}}{l}}\left(\int_{-l}^{l} J(x)\, e^{ikx}\, dx\right) \tag{2.7}$$

and we assume again that $k_0 \neq 0$ and $\hat{J}(k_0) > 0$, $\hat{J}(k_0) \neq \hat{J}(k)\ \forall k = \pm\pi n/l$, $n \in \mathbb{N}$, such that $n \neq n_0$. This is true for functions J as in Figure 2.

Remark 5. In the following sections we analyze the case of spatial and spatio-temporal patterns that occur in the system when, at the most unstable mode $k_0 \neq 0$, either the trace $Tr(\hat{L}(k_0))$ becomes zero, the determinant $\det(\hat{L}(k_0))$ becomes zero, or *both* the trace $Tr(\hat{L}(k_0))$ and the determinant $\det(\hat{L}(k_0))$ become zero at the same value of α.

2.1. Two-population model with adaptation. Here we show that the linearization of the full two-population model does not differ substantially from our fast-inhibition simplification. Reconsider (1.2). Rescale time so that $\tau_E = 1$ and the linearized equations are

$$\begin{aligned}
\frac{du_E}{dt} &= -u_E + \alpha_E(J_{EE} * u_E - J_{EI} * u_I - gA)\,, \\
\tau_I \frac{du_I}{dt} &= -u_I + \alpha_I J_{IE} * u_E\,, \\
\tau_A \frac{dA}{dt} &= -A + u_E\,.
\end{aligned}$$

Here $\alpha_{E,I}$ are the derivatives of $F_{E,I}$ at the constant steady state. As above, the stability is determined by analyzing the eigenvalues of the matrix:

$$M(k) = \begin{pmatrix} -1 + \hat{J}_{EE}(k) & -\hat{J}_{EI}(k) & -g \\ \hat{J}_{IE}(k)/\tau_I & -1/\tau_I & 0 \\ 1/\tau_A & 0 & -1/\tau_A \end{pmatrix},$$

where we have absorbed the parameters $\alpha_{E,I}$ into the $\hat{J}$'s and the parameter g. The eigenvalues of this satisfy a cubic polynomial, $P(\lambda) = \lambda^3 + c_2\lambda^2 + c_1\lambda + c_0$. There is a zero eigenvalue when $c_0 = 0$ and there is an imaginary eigenvalue when $c_1c_2 - c_0 = 0$. For example, the condition for a zero eigenvalue is

$$g = g_{crit} \equiv -1 + (\hat{J}_{EE}(k) - \hat{J}_{EI}(k)\hat{J}_{IE}(k))\,.$$

Note that if we define $\hat{J}(k) = \hat{J}_{EE}(k) - \hat{J}_{EI}(k)\hat{J}_{IE}(k)$, then this is the same condition we obtained in the simpler model. The double zero eigenvalue occurs when both $c_0 = 0$ and $c_1 = 0$, which yields the following condition on the time-constant of adaptation:

$$\tau_A = \frac{1 - \tau_I[\hat{J}_{IE}(k)\hat{J}_{EI}(k)]}{g_{crit}}\,,$$

which, if $\tau_I = 0$, is the same as our earlier condition. The condition for a Hopf bifurcation is more complicated but depends linearly on the degree of adaptation. For small τ_I, it reduces to the conditions above. Thus, for the simple zero and the Takens–Bogdanov bifurcation, the full three-variable model leads to nearly identical conditions on the parameters. The condition for a Hopf bifurcation is more complicated; the following must hold:

$$\begin{aligned}
(\hat{J}(k) - 1 - g)\tau_I\tau_A = {} & [\tau_A + \tau_I - \tau_A\tau_I(1 - \hat{J}_{EE}(k))] \\
& \times [\tau_A\hat{J}(k) - 1 - \tau_A + \tau_I(\hat{J}_{EE}(k) - 1 - g)]\,.
\end{aligned}$$

Note that, like the conditions for the Takens–Bogdanov bifurcation, the quantities depend only on $\hat{J}_{EE}$ and $\hat{J}$, the effective steady-state kernel. As $\tau_I \to 0$, this leads to $-1 + \hat{J}(k) = 1/\tau_A$, which was the condition for the reduced model. Since the linearized behavior of the full three-variable model is similar to that of the simplified system, we compute the normal form only for the simpler system. We expect that there will be little difference in the behavior of the full system.

3. Spatio-temporal patterns obtained by a loss of stability at a purely imaginary pair of eigenvalues. In the case of $Tr(\hat{L}(k_0)) = 0$ and $\det(\hat{L}(k_0)) > 0$, at the most unstable mode k_0 defined by (2.4), or (2.7), with conditions (2.5), (2.6), the eigenvalues of the associated ODE $\frac{d\xi}{dt} = \hat{L}(k_0)\xi$ are complex with zero real part. This happens when the parameters of system (1.3) satisfy

$$g > 1/\tau \quad \text{and} \quad \alpha^* = \frac{1 + 1/\tau}{\hat{J}(k_0)}\,. \tag{3.1}$$

Remark 6. In the following we fix the values of τ and g as above and take α as the bifurcation parameter. The bifurcation value around which we will consider the singular perturbation analysis is α^*. Therefore in the entire section 3, the operator L_0 defined by (2.2), and the matrix $\hat{L}(k)$ defined by (2.3) for all k, where it makes sense, will be evaluated at $\alpha = \alpha^*$.

The matrix $\hat{L}(k_0)$ has purely imaginary eigenvalues $\pm i\omega_0$ with corresponding eigenvectors Φ_0 and $\overline{\Phi}_0$ such that

$$\omega_0 = \frac{1}{\tau}\sqrt{g\tau - 1}\,, \tag{3.2}$$

$$\hat{L}(k_0)\Phi_0 = i\omega_0\Phi_0 \quad \text{with} \quad \Phi_0 = \left(\phi\,,\ \frac{\phi}{1 + i\sqrt{g\tau - 1}}\right)^T. \tag{3.3}$$

Based on the general theory [10], in the case of a pair of purely imaginary eigenvalues that arises at the most unstable mode k_0, the solution U of nonlinear system (1.3) can be approximated by

$$U(x,t) \approx 2\mathrm{Re}\left[z(t)\,\Phi_0\,e^{i(\omega_0 t + k_0 x)} + w(t)\,\Phi_0\,e^{i(\omega_0 t - k_0 x)}\right], \tag{3.4}$$

where z, w are time-dependent functions that satisfy the ODE system

$$\begin{cases} z' = z(a + bz\overline{z} + cw\overline{w})\,, \\ w' = w(a + bw\overline{w} + cz\overline{z}) \end{cases} \tag{3.5}$$

called *the normal form for the Turing–Hopf bifurcation* in the time-and-space-variable case, with $a = a_1 + ia_2$, $b = b_1 + ib_2$, and $c = c_1 + ic_2$ complex coefficients.

The importance of the normal form becomes apparent when we write it in polar coordinates. It provide us with essential information about the existence and stability of the (new) bifurcating solutions. We notice that actually only the signs and values of the real parts a_1, b_1, c_1 of the coefficients a, b, and c play a role in the matter.

In that sense let us define $z(t) = re^{i\theta_1}$ and $w(t) = Re^{i\theta_2}$. Then (3.5) is equivalent to the system $r' = r[a_1 + b_1 r^2 + c_1 R^2]$, $R' = R[a_1 + b_1 R^2 + c_1 r^2]$, $\theta_1' = a_2 + b_2 r^2 + c_2 R^2$,

$\theta_2' = a_2 + b_2R^2 + c_2r^2$, and the normal form is basically reduced to

$$r' = r\,[\,a_1 + b_1r^2 + c_1R^2\,]\,,\quad R' = R\,[\,a_1 + b_1R^2 + c_1r^2\,]\,. \tag{3.6}$$

There are two distinct qualitative pictures of small amplitude bifurcating patterns in a system with normal form (3.5), and so (3.6), as long as $-a_1/b_1 > 0$ and $-a_1/(b_1 + c_1) > 0$ (see Ermentrout [10]).

One corresponds to the solution $\tilde{r} = 0$, $\tilde{R} = \sqrt{-a_1/b_1}$ of (3.6) (or $\tilde{R} = 0$, $\tilde{r} = \sqrt{-a_1/b_1}$) and it represents a traveling periodic wave train with velocity $c = \pm\omega_0/k_0$ ("*traveling wave*"). This can be understood easily by using formula (3.4): Up to a translation in time, an approximation of the solution $U(x,t)$ is then

$$2\sqrt{-a_1/b_1}\mathrm{Re}\left[\Phi_0\, e^{i(\omega_0 t \pm k_0 x)}\right] = 2\sqrt{-a_1/b_1}\mathrm{Re}\left[\Phi_0\, e^{\mp ik_0(ct-x)}\right]. \tag{3.7}$$

Therefore the pattern will change with time and position in space, according to the traveling wave coordinate $\xi = ct - x$ (for an example, see Figure 6).

The other case corresponds to the solution $\tilde{r} = \tilde{R} = \sqrt{-a_1/(b_1 + c_1)}$, and it represents a standing oscillation, periodic in space with spatial frequency k_0, and periodic in time with temporal frequency ω_0 ("*standing wave*"). The approximating solution of $U(x,t)$ (up to a translation in time) is now

$$4\sqrt{-a_1/(b_1 + c_1)}\mathrm{Re}\left[\Phi_0\, e^{i\omega_0 t}\right]\cos(k_0 x)\,, \tag{3.8}$$

and the pattern consists of oscillations with respect to the position x in space for any fixed time t or in oscillations with respect to time at any fixed position x (for an example, see Figure 5).

They cannot be simultaneously stable; therefore, physically, only one of these patterns is selected [10], [9], [12]. The traveling wave solution TW has the corresponding eigenvalues $\lambda_1 = -2a_1$, $\lambda_2 = -\frac{a_1(c_1-b_1)}{b_1}$ with eigenvectors $(1,0)^T$, $(0,1)^T$. Therefore *the traveling wave exists and it is stable* if and only if $a_1 > 0$, $b_1 < 0$, and $c_1 - b_1 < 0$. The standing wave solution SW has the corresponding eigenvalues $\lambda_1 = -2a_1$, $\lambda_2 = -\frac{2a_1(b_1-c_1)}{b_1+c_1}$ with eigenvectors $(1,1)^T$ and $(1,-1)^T$. Therefore *the standing wave exists and it is stable* if and only if $a_1 > 0$, $b_1 + c_1 < 0$, and $c_1 - b_1 > 0$.

We summarize the above observations into the following two theorems.

Theorem 3.1 (existence and stability of traveling and standing waves through a Turing–Hopf bifurcation. See [10]). *Let us consider the normal form* (3.5) *for the Turing–Hopf bifurcation of a nonlinear (time- and one-dimensional-space-dependent) system, and define* $a_1 = Re(a)$, $b_1 = Re(b)$, *and* $c_1 = Re(c)$.

(i) *System* (3.5) *has a TW solution if and only if* $(-a_1)/b_1 > 0$. *Moreover, the TW exists and it is stable if and only if*

$$a_1 > 0\,,\ b_1 < 0\,,\ c_1 - b_1 < 0\,.$$

(ii) *System* (3.5) *has an SW solution if and only if* $(-a_1)/(b_1+c_1)>0$. *Moreover, the SW exists and it is stable if and only if*

$$a_1>0\,,\ b_1+c_1<0\,,\ c_1-b_1>0\,.$$

Theorem 3.2 (see [10]). *Let us assume that a nonlinear (time- and one-dimensional-space-dependent) system passes at the most unstable mode* k_0 *through a Turing–Hopf bifurcation, with eigenvalues* $\pm i\omega_0$ *and eigenvectors* $\Phi_0, \overline{\Phi}_0$. *The associated normal form is* (3.5). *Then*

(i) *the linear approximation of the TW solution is* (3.7). *The velocity of the TW is* $\pm\omega_0/k_0$.

(ii) *The linear approximation of the SW solution is* (3.8).

Since the goal of our study is to investigate the existence of stable TW and/or SW patterns in the neural network (1.3), we have to construct the normal form for the Hopf bifurcation case. More precisely, according to the general theory summarized above, we have to determine the coefficients a, b, and c in (3.5) and then determine their real parts.

3.1. Traveling wave and standing wave patterns in the neural system. The construction of the normal form uses a singular perturbation approach with a proper scaling of the variables, parameters, and time with respect to ϵ, the small pertubation quantity. The Fredholm alternative method is then used to identify solutions for the functional equations obtained from the ϵ-power series expansion.

We include in this section only the main results obtained as a consequence of the construction of the Turing–Hopf bifurcation normal form. A summary of the basic steps of perturbation calculations is then included in Appendix A.

Therefore we are able to compute the expression of the coefficients of the normal form as a dependence on the original parameters of the nonlinear system (1.3). That allows us to identify the regions in the parameter space where stable traveling wave or stable standing wave patterns occur in system (1.3).

We should mention that the numerical simulations of the full nonlinear model around a Hopf bifurcation point indeed showed the presence of stable traveling waves. Nevertheless it was a difficult task to find in simulations the region in the parameter space corresponding to *stable standing waves*. Therefore in this case the analysis is a must. The computed coefficients of the normal form help us to prove the existence of stable standing waves as solutions of the neural system (1.3), and to visualize them numerically.

We state below the results obtained from the normal form calculation.

Theorem 3.3. *If* $g>1/\tau$, *in the neighborhood of the bifurcation value* $\alpha^*=\frac{1+1/\tau}{\hat{J}(k_0)}$, *system* (1.3) *has the normal form* (3.5) *with*

$$a_1=Re(a)=\frac{1}{2}\left[\alpha\,\hat{J}(k_0)-\left(1+\frac{1}{\tau}\right)\right],$$

and $b_1=Re(b)$, $c_1=Re(c)$ *satisfying the equations*

$$b_1=\frac{\tau+1}{4\tau}\,|A|^2\left[F'''(0)+F''(0)^2\cdot\left(-3+\frac{2}{g+1-\frac{(1+1/\tau)\hat{J}(0)}{\hat{J}(k_0)}}+\frac{M_B}{N_B}\right)\right], \tag{3.9}$$

$$c_1+b_1=\frac{\tau+1}{4\tau}\,|A|^2\cdot\Bigg[3\left[F'''(0)-3F''(0)^2\right]$$
$$+F''(0)^2\cdot\left(\frac{2}{g+1-\frac{(1+1/\tau)\hat{J}(2k_0)}{\hat{J}(k_0)}}+\frac{4}{g+1-\frac{(1+1/\tau)\hat{J}(0)}{\hat{J}(k_0)}}+2\frac{M_C}{N_C}+\frac{M_B}{N_B}\right)\Bigg], \tag{3.10}$$

$$c_1-b_1=\frac{\tau+1}{4\tau}\,|A|^2\cdot\Bigg[\left[F'''(0)-3F''(0)^2\right]$$
$$+F''(0)^2\cdot\left(\frac{2}{g+1-\frac{(1+1/\tau)\hat{J}(2k_0)}{\hat{J}(k_0)}}+2\frac{M_C}{N_C}-\frac{M_B}{N_B}\right)\Bigg]. \tag{3.11}$$

Here we have $M_B=M\left(\frac{\hat{J}(2k_0)}{\hat{J}(k_0)}\right)$, $M_C=M\left(\frac{\hat{J}(0)}{\hat{J}(k_0)}\right)$, $N_B=N\left(\frac{\hat{J}(2k_0)}{\hat{J}(k_0)}\right)$, $N_C=N\left(\frac{\hat{J}(0)}{\hat{J}(k_0)}\right)$, *where* M *and* N *are functions defined as*

$$M(X)=(4g\tau-3)[2g\tau-(\tau+1)(\tau+2)]X+4(g\tau-1)(\tau+1)^2+(3g\tau-4-\tau)^2+g\tau(g\tau+\tau-2)$$

and

$$N(X)=(4g\tau-3)(\tau+1)^2X^2+2\tau(\tau+1)(3-g-4g\tau)X+\left[4(g\tau-1)(\tau+1)^2+(3g\tau-4-\tau)^2\right].$$

Based on formulas (3.9), (3.10), (3.11) from Theorem 3.3, we obtain the first important result regarding the type of patterns that can be selected by neural system (1.3).

Theorem 3.4. *Let us assume that the most unstable mode* k_0 *of system* (1.3) *satisfies conditions* (2.5), (2.6), *and at* k_0 *a pair of purely imaginary eigenvalues appears.*

If the firing-rate function F *is such that* $F(0)=0$, $F'(0)>0$, $F''(0)=0$, *and* $F'''(0)<0$, *then system* (1.3) *has a TW and an SW solution for* $\alpha>\alpha^*$, α *close to* α^*. *The SW solution is unstable. The TW solution is stable.*

Proof. First we notice that there exist sigmoid functions F that satisfy the theorem hypotheses. For example, if $\theta=0$, we have from (1.8) $F(u)=\frac{2}{r}\tanh\left(\frac{ru}{2}\right)$, and thus $F(0)=0$, $F'(0)=1$, $F''(0)=0$, $F'''(0)=-\frac{r^2}{2}<0$.

In this case $b_1=\frac{\tau+1}{4\tau}|A|^2F'''(0)<0$, $c_1=2b_1$, and therefore $c_1+b_1<0$ and $c_1-b_1<0$. By Theorem 3.1, both SWs and TWs bifurcate from the trivial solution at $\alpha=\alpha^*$, but only the TWs are stable. ■

Remark 7. Condition $F''(0)=0$ on the firing-rate function is quite restrictive. We are interested in seeing what happens in the general case of $F''(0)\neq 0$ (then the firing-rate function F as in (1.8) has the second and third derivatives $F''(0)=r\frac{1-e^{-r\theta}}{1+e^{-r\theta}}$, $F'''(0)=\frac{r^2\left(e^{-2r\theta}-4e^{-r\theta}+1\right)}{(1+e^{-r\theta})^2}$). In that sense, the coefficients of the normal form (3.5) computed in the previous section provide us with some useful information. They have indeed a complicated expression that does not allow us to give a general, theoretical prediction. Nevertheless we

can use (3.9), (3.10), (3.11) in MATLAB, for example, to search for possible parameter values of g, τ, r, θ, plus coupling J, such that the stable pattern *selected* in the bifurcation at α^* is an SW. The importance of the construction of the normal form (3.5) becomes clear since this allows us to show that *both* TW *and* SW patterns can be found in the neural system (1.3).

Theorem 3.5. *Let us assume that the hypotheses in Theorem 3.3 are true.*

(i) *If $b_1 < 0$ and $c_1 - b_1 < 0$, then for $\alpha > \alpha^*$, sufficiently close to α^*, system (1.3) has a TW solution that is stable. The velocity of the TW is approximately $\left(\pm\frac{\sqrt{g\tau-1}}{\tau k_0}\right)$, and the solution can be approximated by*

$$U(x,t) \approx \sqrt{\frac{2\hat{J}(k_0)(\alpha-\alpha^*)}{(-b_1)}}\, Re\left[\Phi_0 e^{i(\omega_0 t \pm k_0 x)}\right]$$

with Φ_0 and ω_0 defined by (3.2) and (3.3).

(ii) *If $c_1 + b_1 < 0$ and $c_1 - b_1 > 0$, then for $\alpha > \alpha^*$, sufficiently close to α^*, system (1.3) has an SW solution that is stable. The solution can be approximated by*

$$U(x,t) \approx 2\cos(k_0 x)\sqrt{\frac{2\hat{J}(k_0)(\alpha-\alpha^*)}{(-b_1-c_1)}}\, Re\left[\Phi_0 e^{i\omega_0 t}\right].$$

Proof. The proof follows immediately from Theorems 3.2 and 3.3. ∎

Example. If we consider an infinite domain ($l = \infty$), the synaptic coupling J is defined by (1.6) with a graph, as in Figure 1. For example, for $A = 5$, $B = 4$, $a = 1$, $b = 0.3$ we have $k_0 = 1.2967$, $\hat{J}(0) = 1$, $\hat{J}(k_0) = 2.2988$, $\hat{J}(2k_0) = 0.9158$, and at $\tau = 4$ we obtain $\alpha^* = 0.5438$. We choose the function F as in (1.8) with $r = 3$ and $\theta = 0.3$. The theory predicts that there exist values of g such that the stable pattern in neural network (1.3) that occurs through the Hopf bifurcation is the TW, and there exist values of g such that the SW pattern is stable. For example, at $g = 0.34$ both TW and SW bifurcate, but only SW is stable ($b_1 = -0.0651$, $c_1 + b_1 = -0.0955$, $c_1 - b_1 = 0.0347$). On the other hand, at $g = 0.35$ both TW and SW bifurcate, but only TW is stable ($b_1 = -0.1283$, $c_1 + b_1 = -0.2873$, $c_1 - b_1 = -0.0306$).

Remark 8. For the infinite domain problem, the normal form is often formally supplemented with long wave modulation equations. This is a consequence of the fact that, when the bifurcation parameter crosses criticality, an entire *band* of values of the wavenumber k becomes unstable. Formally, a spatial variable $X = \epsilon x$ is introduced and the normal form variables w, z are functions of both the slow time and the slow space scale. The normal form becomes

$$z' = z(a + bz\bar{z} + cw\bar{w}) + dz_{XX} + ew_{XX},$$
$$w' = w(a + bw\bar{w} + cz\bar{z}) + dw_{XX} + ez_{XX},$$

where d, e are complex parameters which depend on the second derivative of the function $\hat{J}(k)$ at the critical wavenumber [17]. These modulation equations are not relevant in the finite size domain since the wavenumbers k take only discrete values.

3.2. Numerical results. A good agreement is obtained between the theoretical prediction (based on the normal form construction) and the numerical simulation of the full nonlinear system (1.3).

For numerical simulations we need to consider a finite domain together with periodic boundary conditions. The synaptic coupling J is defined by (1.7) with a graph as in Figure 2, and there is only a discrete set of wavenumbers. We choose the gain function F as in (1.8) with $r = 3$ and $\theta = 0.3$, or $\theta = 0$, and $l = \pi$ and $a = -0.2$, $b = 2.5$, $c = 2$ in J. Then $k_0 = 1$, $\hat{J}(0) = -0.2$, $\hat{J}(k_0) = 1.25$, $\hat{J}(2k_0) = 1$, and at $\tau = 4$ we obtain $\alpha^* = 1$. The simulations for system (1.3) were run in XPPAUT [7] on a network of 100 neurons, with the method of integration Runge–Kutta RK4 and step size $dt = 0.25$.

At $\theta = 0.3$, the theory predicts that, for example, at $g = 0.45$, both TW and SW bifurcate, but only SW is stable ($b_1 = -3.4412$, $c_1+b_1 = -5.1928$, $c_1-b_1 = 1.6895$). At $g = 0.7$, both TW and SW bifurcate, but only TW is stable ($b_1 = -3.1939$, $c_1+b_1 = -7.7540$, $c_1-b_1 = -1.3661$).

At $\theta = 0$, for any $g > 1/\tau = 0.25$, we can obtain both SW and TW solutions, but the stable pattern is always TW.

These results are confirmed by the numerical simulations of the full model (1.3).

Remark 9. In the figures below we represent the space x on the horizontal axis, the time t on the vertical axis, and the value of the variable $u(x,t)$ by the level of color. The upper left corner corresponds to the minimum value of x that increases to the right. The value of time increases in the up-to-down direction. In general, the time is represented after $t = 3000$ transients. We choose two different sets of initial conditions to illustrate the possible behaviors in system (1.3).

Let us consider first the case $\theta = 0.3$.

For different values of the parameter g, e.g., $g = 0.45$ and $g = 0.7$, before the bifurcation point, at $\alpha = 0.99$, by choosing random initial conditions around the origin, the solution decays in time to zero. After the bifurcation point, at $\alpha = 1.01$, both TW and SW patterns can be obtained, depending on the choice of the initial conditions. In order to test which pattern is stable, we have also run the simulations of system (1.3) in the presence of white noise added to the first equation and scaled by a factor of 0.001 (see Figures 4(b)–7(b)).

As a consequence we notice that at $g = 0.45$, the stable pattern is SW (see Figures 4 and 5), and at $g = 0.7$ the stable pattern is TW (see Figures 6 and 7). This means that for both sets of initial conditions—that in the absence of noise might produce different patterns—we obtain *the same pattern in the presence of noise*, that is, SW at $g = 0.45$, respectively, TW at $g = 0.7$.

At $\theta = 0$ the stable pattern obtained as a result of added noise is always TW. We present the numerical results in Figures 8 and 9 for $g = 0.45$, and in Figures 10 and 11, respectively, for $g = 0.7$.

3.3. Summary. We have shown that with strong adaptation, $g\tau > 1$, spatio-temporal patterns bifurcate from the uniform resting state. Depending on the position of the rest state relative to the inflection point of the sigmoid nonlinearity, we can get either TWs or standing oscillations. The latter were not found in the model of Hansel and Sompolinsky (or at least they were not discussed). Ermentrout [10] found both TWs and SWs in the Wilson–Cowan equations but did not compute the normal forms needed to specify which were stable.

The biological interpretation of the TWs is fairly clear. There are many examples of such TWs in experimental preparations. These are reviewed and their possible functional role is discussed in [13]. SWs are more difficult to find in experimental preparations. However, suppose that we view the model in the manner of Hansel and Sompolinsky, where the spatial

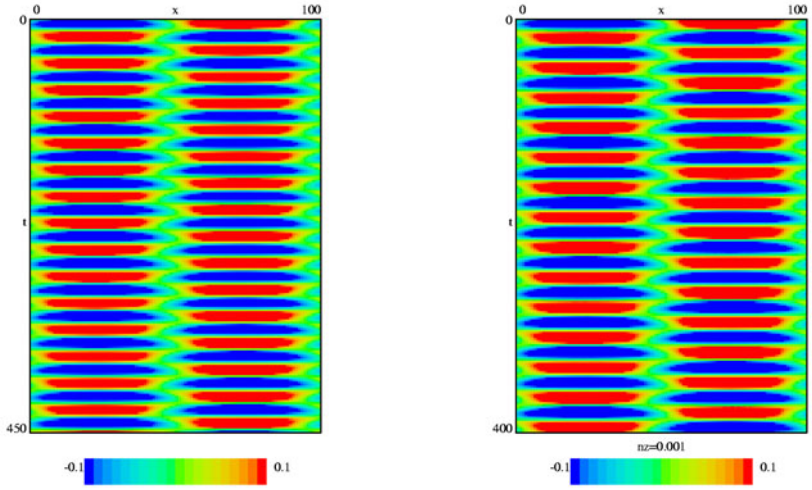

Figure 4. (a) *SW is the pattern obtained at* $g = 0.45$, $\theta = 0.3$, *and set* 1 *of initial conditions.* (b) *In the presence of noise, SW is preserved.*

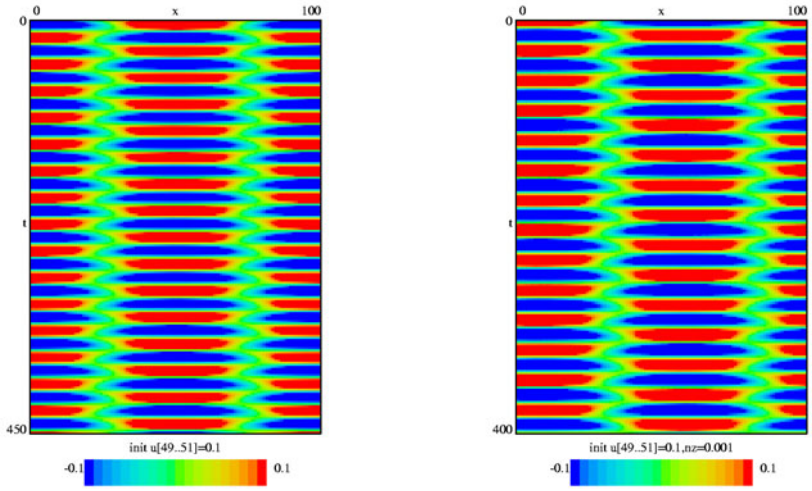

Figure 5. (a) *SW is the pattern obtained at* $g = 0.45$, $\theta = 0.3$, *and set* 2 *of initial conditions.* (b) *It is stable since in the presence of noise, SW is preserved.*

variable x represents the orientation tuning of a cell. Suppose that the critical wavenumber is 1 so that the SW solution has the form $\cos \omega t \cos 2\pi x/L$. This represents two groups of cells whose preferred orientations are mutually orthogonal; when one group is at its maximum, the other is at its minimum. Solutions of this form have been posited as neural analogues of

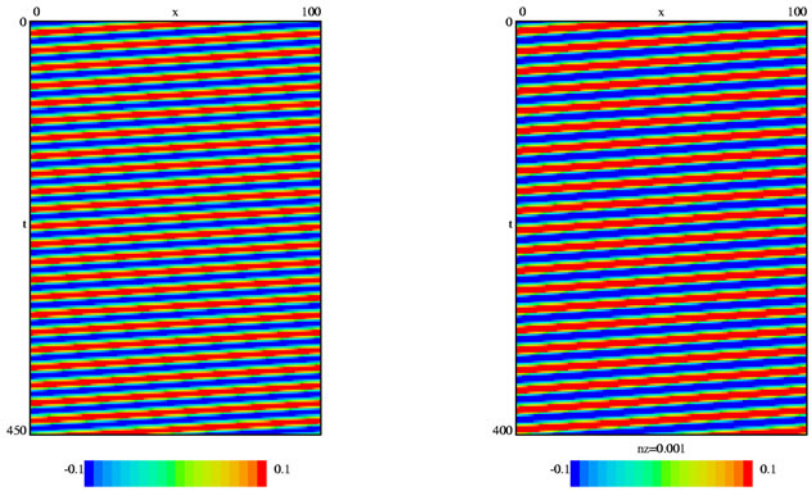

Figure 6. (a) *TW is the pattern obtained at* $g = 0.7$, $\theta = 0.3$, *and set* 1 *of initial conditions.* (b) *In the presence of noise, TW is preserved.*

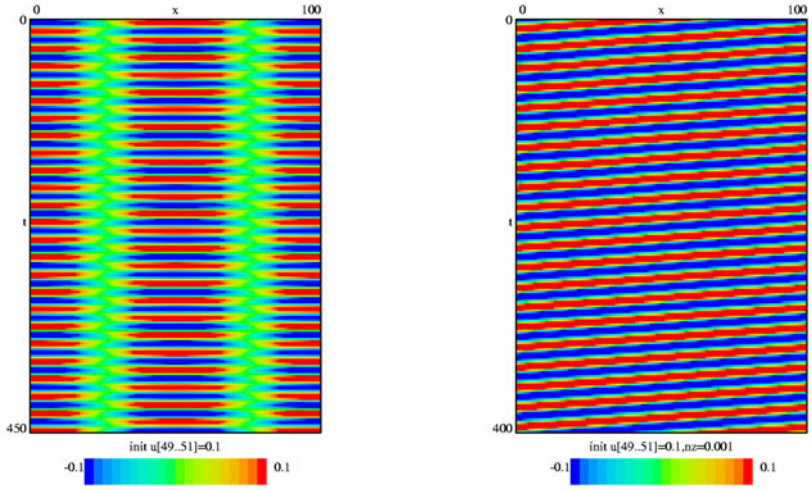

Figure 7. (a) *SW is the pattern obtained at* $g = 0.7$, $\theta = 0.3$, *and set* 2 *of initial conditions.* (b) *It is unstable since in the presence of noise, SW is replaced by TW.*

perceptual reversals [23] and binocular rivalry [18].

4. Spatial patterns obtained by a loss of stability at zero eigenvalue. The case when the determinant vanishes first and the trace is still negative is analyzed in this section. It

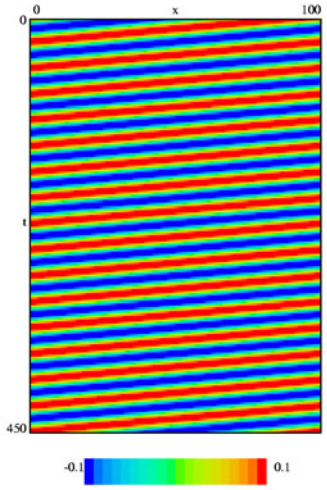

Figure 8. *TW is the pattern obtained at $g = 0.45$, $\theta = 0$, and set 1 of initial conditions.*

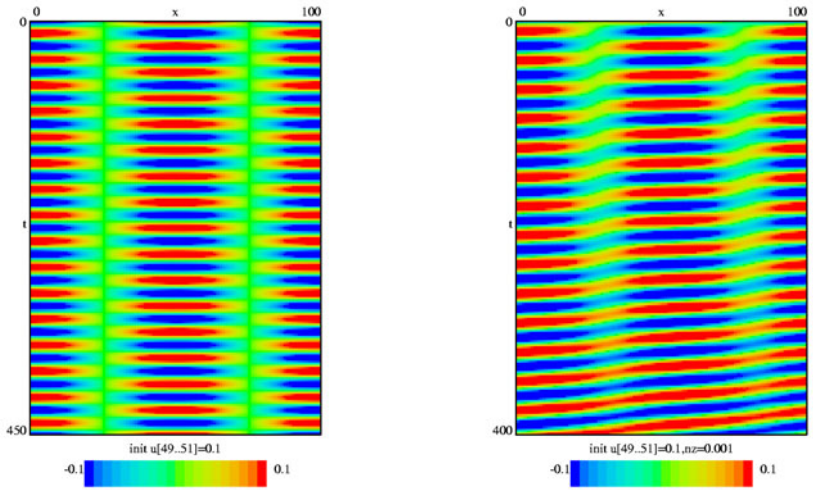

Figure 9. (a) *SW is the pattern obtained at $g = 0.45$, $\theta = 0$, and set 2 of initial conditions.* (b) *It is unstable since in the presence of noise, SW is replaced by TW.*

corresponds to a choice of parameters of system (1.3) satisfying the following conditions:

$$g < 1/\tau \quad \text{and} \quad \alpha^* = \frac{g+1}{\hat{J}(k_0)}. \tag{4.1}$$

At the most unstable mode k_0 we have $\det(\hat{L}(k_0)) = 0$ and $Tr(\hat{L}(k_0)) < 0$; therefore the

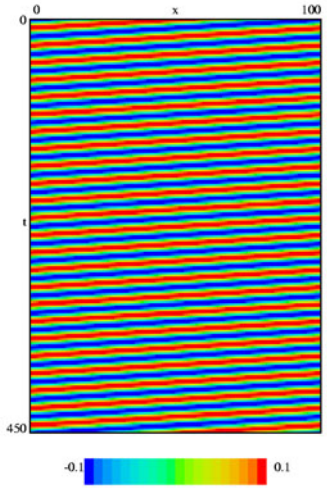

Figure 10. *TW is the pattern obtained at $g = 0.7$, $\theta = 0$, and set 1 of initial conditions.*

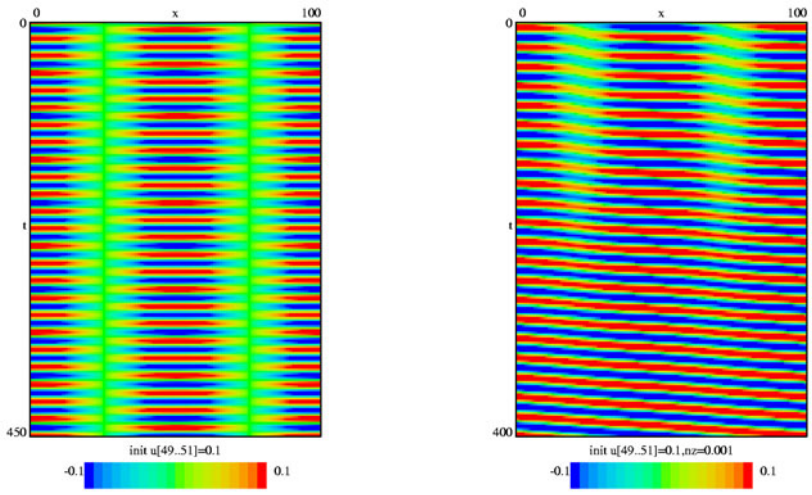

Figure 11. (a) *SW is the pattern obtained at $g = 0.7$, $\theta = 0$, and set 2 of initial conditions.* (b) *It is unstable since in the presence of noise, SW is replaced by TW.*

associated ODE system $\frac{d\xi}{dt} = \hat{L}(k_0)\xi$ has a simple zero eigenvalue with eigenvector Φ_0 defined by $\hat{L}(k_0)\Phi_0 = \mathbf{0}$, that is, for example, $\Phi_0 = (1,1)^T$. Let us consider also the eigenvector Ψ_0 of the adjoint equation $\hat{L}(k_0)^T\Psi_0 = \mathbf{0}$ such that $\Phi_0 \cdot \Psi_0 = 1$. Then we have $\Psi_0 = \frac{1}{1-g\tau}(1,-g\tau)^T$.

The pattern that results through the bifurcation at a simple zero eigenvalue oscillates with respect to space position due to the unstable mode k_0, but it is independent of time (the

details of the construction of the normal form are given in Appendix A). We call this pattern *steady state* or *stationary pattern*.

Theorem 4.1. *If $g < 1/\tau$, in the neighborhood of the bifurcation value $\alpha^* = \frac{g+1}{\hat{J}(k_0)}$, system (1.3) has the normal form*

$$z' = \eta_1 z + \Lambda |z|^2 z \tag{4.2}$$

with $\eta_1 = \frac{\alpha \hat{J}(k_0) - (g+1)}{1-g\tau}$ and coefficient

$$\begin{aligned} \Lambda = & \frac{1}{2(1-g\tau)} \left[F'''(0) - 3F''(0)^2 \right] \\ & + \frac{F''(0)^2}{(1-g\tau)(g+1)} \cdot \left[\frac{\hat{J}(k_0)}{\hat{J}(k_0) - \hat{J}(0)} + \frac{\hat{J}(k_0)}{2[\hat{J}(k_0) - \hat{J}(2k_0)]} \right]. \end{aligned} \tag{4.3}$$

Theorem 4.2. *In the hypotheses of Theorem 4.1, the SS solution that occurs about the bifurcation point $\alpha^* = \frac{g+1}{\hat{J}(k_0)}$ has the following first order approximation:*

$$SS: \; u(x,t) = v(x,t) \approx 2 \cos(k_0 x) \sqrt{\frac{\alpha \hat{J}(k_0) - (g+1)}{(1-g\tau)(-\Lambda)}}. \tag{4.4}$$

SS is stable if and only if $\Lambda < 0$ and $\alpha > \alpha^*$.

Proof. In polar coordinates $z = r\, e^{i\theta_1}$, the normal form equivalent to (4.2) is $r' = r(\eta_1 + \Lambda r^2)$, $\theta_1' = 0$. A nonzero solution exists only in the case $\eta_1 \Lambda < 0$ and it is $\tilde{r} = \sqrt{\frac{\eta_1}{-\Lambda}}$ and θ_1 a constant.

The first order approximation of the nontrivial solution $U(x,t)$ is then

$$U(x,t) \approx z(t)\Phi_0 e^{ik_0 x} + \overline{z}(t)\Phi_0 e^{-ik_0 x} = 2\Phi_0 \mathrm{Re}\left[z(t)\, e^{ik_0 x} \right] = 2\sqrt{\frac{\eta_1}{-\Lambda}} \Phi_0 \cos(k_0 x + \theta_1).$$

Since $\Phi_0 = (1,1)^T$, we obtain exactly (4.4) up to a translation in space.

The stability condition comes from $h'(\tilde{r}) = -2\eta_1 < 0$, where $h(r) = r(\eta_1 + \Lambda r^2)$, together with the existence condition $\eta_1 \Lambda < 0$. ∎

We note that if the parameter θ in the firing-rate function F from (1.8) is $\theta = 0$, we obtain $F''(0) = 0$, $F'''(0) < 0$. Then $\Lambda < 0$ and the pitchfork bifurcation is supercritical: a (stable) stationary pattern occurs for $\alpha > \frac{g+1}{\hat{J}(k_0)}$.

5. Spatio-temporal patterns obtained by a loss of stability at a double-zero eigenvalue.

In the previous sections, we analyzed bifurcation to TWs and SWs when $g\tau > 1$ (strong adaptation) and to stationary patterns when $g\tau < 1$ (weak adaptation). The former (resp., latter) patterns occur when the trace becomes positive at a lower (resp., higher) value of α than at which the determinant becomes negative. We note that, in both cases, the normal form is no longer defined in the limit as $g\tau \to 1$; for the Hopf case, $\omega_0 \to 0$; and in the simple zero eigenvalue case, the coefficients of the normal form become unbounded.

An obvious question is how these possible patterns in system (1.3) interact, that is, how the system's behavior changes from TW or SW to a stationary pattern or vice versa. The

transition between spatio-temporal and only spatial patterns can be analyzed by a study of the case when the trace and the determinant of the linearized system vanish simultaneously. Then at the most unstable mode we obtain a double-zero eigenvalue. The double-zero eigenvalue case is approached from two different directions: one in which we already have a zero eigenvalue and now obtain another (that is, coming from the domain of spatial/stationary patterns), and another in which we have a pair of purely imaginary eigenvalues $\pm i\omega_0$ that collide (that is, coming from the domain of spatio-temporal patterns).

As a result of the above remarks, the aim of the present section is to study behavior in system (1.3) at the transition between stationary states and TWs/SWs. Therefore we assume that at the most unstable mode k_0 we have $Tr(\hat{L}(k_0)) = \det(\hat{L}(k_0)) = 0$. This is true when the parameters satisfy the conditions

$$g^* = 1/\tau \quad \text{and} \quad \alpha^* = \frac{1 + 1/\tau}{\hat{J}(k_0)}\,. \tag{5.1}$$

Remark 10. In the following we fix the value of τ and take α and g as bifurcation parameters. The bifurcation values around which we will consider the singular perturbation analysis are α^* and g^*. Therefore in the entire section 5, the operator L_0 defined by (2.2), and the matrix $\hat{L}(k)$ defined by (2.3) for all k, where it makes sense, will be evaluated at $\alpha = \alpha^*$ and $g = g^*$.

At $\pm k_0$ the associated ODE $\frac{d\xi}{dt} = \hat{L}(k_0)\xi$ has a double-zero eigenvalue. For all other values $k \neq \pm k_0$ we have $Tr(\hat{L}(k)) < 0$ and $\det(\hat{L}(k)) > 0$, and the corresponding eigenvalues have negative real part.

Let us construct the (generalized) eigenvectors of $\hat{L}(k_0)$ and $\hat{L}(k_0)^T$ as follows:

$$\Phi_0 = \frac{1}{\sqrt{\tau}}\begin{pmatrix}1\\1\end{pmatrix},\ \Psi_1 = \frac{1}{\sqrt{\tau}}\begin{pmatrix}1\\-1\end{pmatrix},\ \Phi_1 = \sqrt{\tau}\begin{pmatrix}1\\0\end{pmatrix},\ \Psi_0 = \sqrt{\tau}\begin{pmatrix}0\\1\end{pmatrix}, \tag{5.2}$$

according to the conditions

$$\begin{cases} \hat{L}(k_0)\Phi_0 = \mathbf{0}\,,\ \hat{L}(k_0)\Phi_1 = \Phi_0\,,\ \hat{L}(k_0)^T\Psi_1 = \mathbf{0}\,,\ \hat{L}(k_0)^T\Psi_0 = \Psi_1\,, \\ \Phi_0 \cdot \Psi_0 = \Phi_1 \cdot \Psi_1 = 1\,,\ \Phi_0 \cdot \Psi_1 = \Phi_1 \cdot \Psi_0 = 0\,. \end{cases} \tag{5.3}$$

Around the double-zero bifurcation point, the first order approximation of the solution of nonlinear system (1.3) is given by its projection on the generalized eigenspace. That means U can be approximated by

$$U(x,t) \approx 2\mathrm{Re}\left[z(t)\,\Phi_0\,e^{ik_0x} + w(t)\,\Phi_1\,e^{ik_0x}\right], \tag{5.4}$$

where z, w are time-dependent functions that satisfy the ODE system with real coefficients

$$\begin{cases} z' = w\,, \\ w' = \zeta_1 z + \zeta_2 w + A|z|^2 z + Cz[\,\overline{z}\,w + z\,\overline{w}\,] + D|z|^2 w\,, \end{cases} \tag{5.5}$$

called *the normal form for the double-zero (Takens–Bogdanov) bifurcation with $O(2)$-symmetry* [6].

Indeed the linear part of system (5.5) has two zero eigenvalues when the parameters $\zeta_1 = 0$ and $\zeta_2 = 0$. That is why we call this type of bifurcation "double-zero" or "Takens–Bogdanov." The additional name of "$O(2)$-symmetry" comes from the fact that system (5.5) exhibits symmetry under both rotations and reflections. This means that the vector field $G(z, w)$ (the right-hand side of (5.5)) commutes with the rotation $z \mapsto e^{i\theta} z$ for any angle $\theta \in \mathbb{R}$, i.e., we have $G(e^{i\theta} z, e^{i\theta} w) = e^{i\theta} G(z, w)$, and it also commutes with reflection $z \mapsto \overline{z}$, i.e., $G(\overline{z}, \overline{w}) = \overline{G(z, w)}$. Therefore the system shows no directional preference and we say that it is *isotropic*. The technical terminology is that the vector field G, and therefore system (5.5), is covariant (or equivariant) with respect to the group $O(2)$ of rotations and reflections.

Recall that for (1.3) we seek spatially periodic solutions of the form $\psi_k\, e^{ikx} + cc$, where cc stands for the complex conjugate of the previous term.

Since $\left[\psi_k\, e^{ik(x+d)} + cc = e^{ikd}\psi_k\, e^{ikx} + cc\right]$, a translation in space $[x \mapsto x+d]$ will be associated with a rotation of the time-dependent vector ψ_k. Furthermore, a reflection in space $[x \mapsto (-x)]$ is associated with a reflection of the vector ψ_k since $\left[\psi_k\, e^{ik(-x)} + cc = \overline{\psi}_k\, e^{ikx} + cc\right]$. We note that the vector field of original system (1.3) satisfies properties $G(\,u(x+d,t), v(x+d,t)\,) = G(u,v)(x+d,t)$ and $G(\,u(-x,t), v(-x,t)\,) = G(u,v)(-x,t)$, so we say that system (1.3) is isotropic.

System (1.3) has at least one solution that preserves the symmetry with respect to both rotations, $u(x+d,t) = e^{ikd}u(x,t)$, $v(x+d,t) = e^{ikd}v(x,t)$, and reflection $u(-x,t) = \overline{u(x,t)}$, $v(-x,t) = \overline{v(x,t)}$, and this is the trivial solution $u(x,t) = v(x,t) \equiv 0$. For different values of parameters, other solutions may exist which do not necessarily preserve the symmetry. We say that the symmetry in the system is broken and call the phenomenon that leads to this situation *symmetry breaking bifurcation*. The above-mentioned correspondence between (1.3) and (5.5), together with formula (5.4), allows us to work with system (5.5) and detect the solutions that break its symmetry, rather than working with (1.3).

Dangelmayr and Knobloch present in [6] a detailed analysis of the existence and stability properties for five types of possible solutions of system (5.5). These are the trivial solution/T, steady state/SS, traveling wave/TW, standing wave/SW, and modulated wave/MW. Depending on the sign of the coefficient A, and then the signs of D and $M = 2C + D$, together with some nondegeneracy conditions based on the value of the ratio D/M, different regions in the parameter plane (ζ_1, ζ_2) were identified, and the corresponding bifurcation diagrams were drawn. That is, as a dependence on the values of parameters, all possible qualitatively different behaviors in the system are described.

As an example, TWs break the symmetry with respect to reflection and keep the symmetry to rotations. On the other hand, SWs break the symmetry with respect to rotations but keep the symmetry to reflection (see below).

We summarize in the following the basic ideas followed by Dangelmayr and Knobloch [6] in their analysis. Moreover, in a similar approach to section 3 we give a geometric interpretation of the solutions SS, TW, SW, and MW.

First we write z and w in polar coordinates and transform system (5.5) accordingly. Since $w = z'$ we need only the polar representation of z, say $z(t) = r\,e^{i\phi}$. Then by the separation of the real and imaginary parts, system (5.5) is equivalent to

$$\begin{cases} r'' - r(\phi')^2 - r(\zeta_1 + Ar^2) - r'\,(\zeta_2 + Mr^2) = 0\,, \\ r\,\phi'' + 2r'\phi' - r\,\phi'\,(\zeta_2 + Dr^2) = 0\,. \end{cases} \tag{5.6}$$

The trivial solution T corresponds to the solution $r = 0$ and exists for all parameter values. Therefore $z(t) = w(t) = 0$ and from (5.4) we have $U(x,t) \equiv 0$. The solution is independent of time and position in space.

The linearization of (5.6) around $r = 0$, $\phi' = 0$, e.g., take $r = 0 + \xi$, $\phi' = 0 + \eta$ with ξ, η small, is the equation $\xi'' - \zeta_2\,\xi' - \zeta_1\,\xi = 0$. The eigenvalues have negative real part if and only if $\zeta_1 < 0$ and $\zeta_2 < 0$. The stability of the trivial solution T is lost at $\zeta_1 = 0$ through a zero eigenvalue when other constant solutions r_0 appear (with ϕ' still zero) (we denote the line $\zeta_1 = 0$ in the parameter space (ζ_1, ζ_2) by L_0; see Figure 12), or at $\zeta_2 = 0$ and $\zeta_1 < 0$ (see the half-line H_0 in Figure 12) through a pair of purely imaginary eigenvalues $\pm i\omega_0$, when a small amplitude periodic solution $r = r(t)$ appears with ϕ' still zero. This case will correspond to an SW solution. We mention that the $O(2)$-symmetry of the system forces both TW and SW solutions to appear simultaneously from the trivial solution.

The SS corresponds to solution of (5.6) *constant on the radial direction*, $r(t) = r_0$, and *with no orbital motion* $\phi' = 0$. This means that r_0 must satisfy the condition $\zeta_1 + Ar_0^2 = 0$ and that, obviously, it does not exist for all parameter values. In order to get an SS we need $A\zeta_1 < 0$ so that $r_0 = \sqrt{-\zeta_1/A}$. Moreover, $\phi' = 0$ implies $\phi(t) = \omega$, constant, and $z(t) = r_0\,e^{i\omega}$, $w(t) = z'(t) = 0$. The approximating formula (5.4) implies $U(x,t) = 2r_0\Phi_0\cos(k_0x + \omega) = 2\sqrt{-\frac{\zeta_1}{A}}\Phi_0\cos(k_0x + \omega)$, or up to a translation in space,

$$U(x,t) \approx 2\sqrt{-\frac{\zeta_1}{A}}\,\cos(k_0x)\,\Phi_0\,. \tag{5.7}$$

The SS pattern consists of oscillations with respect to the position in space x, and it is independent of time; therefore it forms stationary stripes (see Figure 19 for an example).

The linearization of (5.6) around $r = r_0$, $\phi' = 0$, e.g., take $r = r_0 + \xi$, $\phi' = 0 + \eta$ with ξ, η small, is the system of equations $\xi'' - (\zeta_2 + Mr_0^2)\,\xi' - 2Ar_0^2\,\xi = 0$, $\eta' - (\zeta_2 + Dr_0^2)\eta = 0$, i.e., $\xi'' - (\zeta_2 - \frac{M}{A}\zeta_1)\xi' + 2\zeta_1\xi = 0$ and $\eta' - (\zeta_2 - \frac{D}{A}\zeta_1)\eta = 0$. The only possible bifurcations that result in appearance/disappearance of time-independent solutions correspond to a zero eigenvalue. That can happen for $\zeta_1 = 0$ (we have already mentioned this case of a new SS branch solution) or for $A\zeta_2 = D\zeta_1$, $A\zeta_1 < 0$ (see the half-line L_m in Figure 12) when a new ϕ' constant and nonzero solution is created, say $\phi' = \omega_0$ (see the TW case).

The TW corresponds to a solution of (5.6) *constant on the radial direction*, $r(t) = r_0$, but *with orbital motion with constant angular frequency* $\phi' = \omega_0$. This means that r_0 and ω_0 must satisfy the conditions $\zeta_2 + Dr_0^2 = 0$ and $\omega_0^2 = -(\zeta_1 + Ar_0^2)$ and TW exists only in the parametric regime $D\zeta_2 < 0$, $\frac{A}{D}\zeta_2 - \zeta_1 > 0$. We have $r_0 = \sqrt{-\zeta_2/D}$ and $\omega_0 = \pm\sqrt{A\zeta_2/D - \zeta_1}$; then $z(t) = r_0\,e^{i(\omega_0 t + \omega)}$, $w(t) = z'(t) = ir_0\omega_0\,e^{i(\omega_0 t + \omega)}$ and from formula (5.4), the TW equation, up to a translation in space, is

$$U(x,t) \approx 2\sqrt{-\frac{\zeta_2}{D}}\,\mathrm{Re}\left[(\Phi_0 + i\omega_0\Phi_1)\,e^{i(\omega_0 t + k_0 x)}\right], \tag{5.8}$$

with

$$\omega_0 = \pm\sqrt{\frac{A}{D}\zeta_2 - \zeta_1}\,. \tag{5.9}$$

The TW solution changes with respect to time and position in space according to the TW coordinate $\xi = ct - x$, where $c = \omega_0/k_0$ is the wave velocity; therefore the pattern is formed by nonstationary stripes, i.e., stripes with finite slope (see Figure 16 for an example). Equation (5.8) shows that TW solutions break reflection symmetry but respect the symmetry to rotations.

The MW corresponds to a periodic solution $r(t)$ of (5.6) and a nonzero angular velocity ϕ'. This means that we have *oscillations in the radial direction* and *orbital motion* as well. The MWs bifurcate from a TW through another Hopf bifurcation that introduces a new frequency in the solution. Therefore the MW pattern is characterized by two different frequencies, one corresponding to the orbital motion and the other to radial oscillations (not shown in this paper).

The SW corresponds to a periodic solution $r(t)$ of (5.6) and $\phi' = 0$. This means that we have *oscillations in the radial direction* and *no orbital motion*. SWs can occur as oscillations about the trivial solution or about an SS. From (5.6), $r(t)$ satisfies the equation $r'' - r'(\zeta_2 + Mr^2) - r(\zeta_1 + Ar^2) = 0$ and $\phi = \omega$ is constant. Then $z(t) = r(t)\,e^{i\omega}$, $w(t) = z'(t) = r'(t)\,e^{i\omega}$, and (5.4) implies, up to a translation in space,

$$U(x,t) \approx 2\big[r(t)\,\Phi_0 + r'(t)\,\Phi_1\big]\,\cos(k_0 x)\,, \tag{5.10}$$

where $r(t)$ is the periodic solution of period, say, $2\pi/\omega_0$ of the ODE

$$r'' - r'(\zeta_2 + Mr^2) - r(\zeta_1 + Ar^2) = 0\,. \tag{5.11}$$

The SW solution oscillates with respect to time with frequency ω_0 for any fixed position in space and oscillates with respect to space with frequency k_0 for any fixed t (see Figure 17 for an example of the SW pattern). Equation (5.10) shows that SW solutions break rotation symmetry but respect the symmetry to reflection.

Remark 11. We summarized above the properties of possible patterns in a system with $O(2)$-symmetry. Let us describe now the type of bifurcation diagram [6] that we will need later in our study. It corresponds to $A < 0$ with $D < 0$, $M < 0$, and $0 < D/M < \frac{1}{2}$. The parameter plane (ζ_1, ζ_2) is divided into seven regions (see Figure 12) by the following curves: $L_0 : \zeta_1 = 0$, $H_0 : [\zeta_2 = 0,\ \zeta_1 < 0]$, $L_M : [A\zeta_2 = M\zeta_1,\ \zeta_1 > 0]$, $SL_S : [5A\zeta_2 = 4M\zeta_1,\ \zeta_1 > 0]$, $SN_{S2} : [A\zeta_2 \approx 0.74M\zeta_1,\ \zeta_1 > 0]$, $L_m : [A\zeta_2 = D\zeta_1,\ \zeta_1 > 0]$. A bifurcation producing SS solutions occurs along L_0, and a Hopf bifurcation, from the trivial solution T, of a TW and SW_1 occurs along H_0. By crossing L_M, SL_S, SN_{S2}, and L_m secondary bifurcations occur: along SN_{S2} we have a saddle-node for two SWs, SW_1 and SW_2; along L_M an SW oscillation SW_3 about a nontrivial SS bifurcates; then SW_3 and SW_2 undergo a global bifurcation and join smoothly to each other along SL_S; and TW bifurcates from an SS along L_m.

Since our goal is to study how the SS, TW, and SW solutions occur in the neural system (1.3) and how they interact, that is, how the patterns change as the parameters α and g vary about α^* and g^*, the next necessary step in the analysis is to construct the normal form for the double-zero bifurcation and determine its coefficients. That is the aim of the next section.

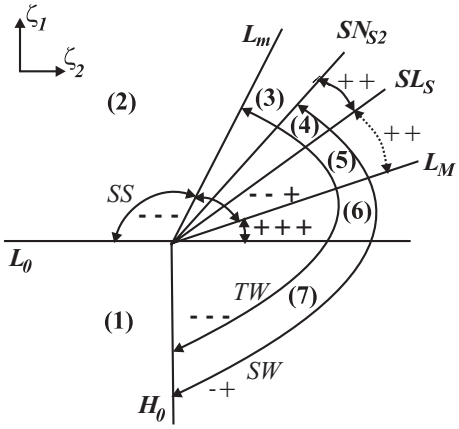

Figure 12. *The bifurcation diagram corresponding to system (5.5) with $A < 0$, $D < 0$, $M < 0$, and $0 < D/M < 1/2$.*

5.1. Double-zero bifurcation with $O(2)$-symmetry and pattern formation. In this section we construct the normal form for the double-zero bifurcation with $O(2)$-symmetry for neural system (1.3) (see Appendix A for details) and delineate the regions in the parameter space that corresponds to different possible scenarios.

We obtain the following results.

Theorem 5.1. *For any positive τ, in the neighborhood of the bifurcation values $\alpha^* = \frac{1+1/\tau}{\hat{J}(k_0)}$ and $g^* = 1/\tau$, system (1.3) has the normal form (5.5) with $\zeta_1 = \frac{\alpha\,\hat{J}(k_0)-(g+1)}{\tau}$, $\zeta_2 = \alpha\,\hat{J}(k_0) - (1+\frac{1}{\tau})$, and the coefficients*

$$\begin{cases} A = \frac{1}{2\tau^2}[F'''(0) - 3F''(0)^2] + \frac{F''(0)^2}{\tau(\tau+1)} \cdot \left[\frac{\hat{J}(k_0)}{\hat{J}(k_0)-\hat{J}(0)} + \frac{\hat{J}(k_0)}{2\,[\,\hat{J}(k_0)-\hat{J}(2k_0)\,]}\right], \\ C = (\tau+1)A + \frac{F''(0)^2}{\tau(\tau+1)} \cdot \frac{\hat{J}(k_0)}{\hat{J}(k_0)-\hat{J}(0)}, \\ D = (\tau+1)A + \frac{F''(0)^2}{\tau(\tau+1)} \cdot \frac{\hat{J}(k_0)}{\hat{J}(k_0)-\hat{J}(2k_0)}. \end{cases}$$

Theorem 5.2. *In the hypotheses of Theorem 5.1, the SS, TW, and SW solutions that occur about the bifurcation point $\alpha^* = \frac{1+1/\tau}{\hat{J}(k_0)}$ and $g^* = 1/\tau$ are approximated by the following expressions:*

$$SS:\ u(x,t) = v(x,t) \approx \frac{2}{\tau}\cos(k_0 x)\sqrt{\frac{\alpha\,\hat{J}(k_0)-(g+1)}{(-A)}},$$

$$TW:\ \begin{cases} u(x,t) \approx [\,\cos(\omega_0 t + k_0 x) - \tau\,\omega_0 \sin(\omega_0 t + k_0 x)\,]\sqrt{\frac{2[\alpha\,\hat{J}(k_0)-(1+1/\tau)]}{(-D)\,\tau}}, \\ v(x,t) \approx \cos(\omega_0 t + k_0 x)\sqrt{\frac{2[\alpha\,\hat{J}(k_0)-(1+1/\tau)]}{(-D)\,\tau}}, \end{cases}$$

$$SW:\ \begin{cases} u(x,t) \approx \frac{2}{\sqrt{\tau}}\,[\,r(t) + \tau\,r'(t)\,]\,\cos(k_0 x), \\ v(x,t) \approx \frac{2}{\sqrt{\tau}}\,r(t)\,\cos(k_0 x), \end{cases}$$

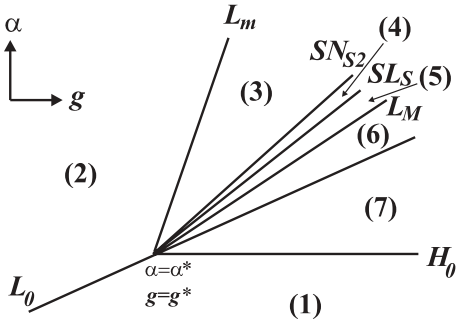

Figure 13. *The bifurcation diagram corresponding to system (1.3) about (α^*, g^*) when $\theta = 0$ in F.*

where $r(t)$ is the periodic solution of

$$r'' - r'\left[[\alpha\,\hat{J}(k_0) - (1+1/\tau)] + (2C+D)r^2\right] - r\left[\frac{\alpha\,\hat{J}(k_0) - (g+1)}{\tau} + Ar^2\right] = 0$$

and

$$\omega_0 = \pm\sqrt{\frac{A}{D}[\alpha\,\hat{J}(k_0) - (1+1/\tau)] - \frac{1}{\tau}[\alpha\,\hat{J}(k_0) - (g+1)]}\,.$$

Proof. The above formulas result directly from (5.7), (5.8), and (5.10) with Φ_0 and Φ_1 defined by (5.2) and ζ_1, ζ_2 as in Theorem 5.1. ■

Theorem 5.3. *Let us assume that the most unstable mode k_0 of system (1.3) satisfies conditions (2.5), (2.6), and at k_0 a double-zero eigenvalue occurs.*

If the firing-rate function F is such that $F(0) = 0$, $F'(0) > 0$, $F''(0) = 0$, and $F'''(0) < 0$, then about $\alpha^* = \frac{1+1/\tau}{\hat{J}(k_0)}$, $g^* = 1/\tau$, system (1.3) has the bifurcation diagram from Figure 13 (equivalent to Figure 12). The curves that divide the parametric plane (α, g) into seven regions have the following equations:

$$\text{(5.12)}\qquad \begin{cases} L_0 \,:\, \alpha\,\hat{J}(k_0) = g+1\,, \\ H_0 \,:\, \alpha\,\hat{J}(k_0) = 1+1/\tau\,,\ g > 1/\tau\,, \\ L_M \,:\, \alpha\,\hat{J}(k_0) = \frac{\tau+1}{2\tau+3}(3g+2)\,,\ g > 1/\tau\,, \\ SL_S \,:\, \alpha\,\hat{J}(k_0) = \frac{\tau+1}{7\tau+12}(12g+7)\,,\ g > 1/\tau\,, \\ SN_{S2} \,:\, \alpha\,\hat{J}(k_0) \approx \frac{\tau+1}{61\tau+111}(111g+61)\,,\ g > 1/\tau\,, \\ L_m \,:\, \alpha\,\hat{J}(k_0) = (\tau+1)g\,,\ g > 1/\tau\,. \end{cases}$$

Proof. Since $F''(0) = 0$ and $F'''(0) < 0$, we have $A < 0$, $C = D = (\tau+1)A < 0$ and then $M < 0$, $D/M = \frac{1}{3} \neq \frac{1}{2}, \frac{3}{5}, 0.7, 0.74, \frac{3}{4}, \frac{4}{5}, 1$ (the nondegeneracy conditions). This is exactly the case described by Figure 12. With the formulas provided by Theorem 5.1 we obtain immediately (5.12). ■

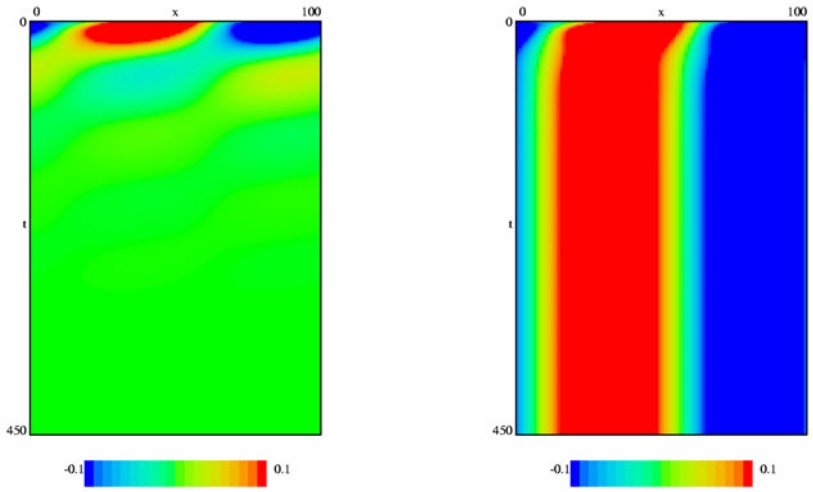

Figure 14. *Along the bifurcation line L_0 we have* (a) *the trivial solution T in region* (1)*, at $\alpha = 0.95$, $g = 0.2$, and* (b) *SS in region* (2)*, at $\alpha = 0.98$, $g = 0.2$. The same set of initial conditions Ic1 is used.*

5.2. Numerical results. We run the numerical simulations for the same hypotheses as in section 3.2. The full system (1.3) is simulated with synaptic coupling (1.7) that has the coefficients $a = -0.2$, $b = 2.5$, $c = 2$; the gain function F is chosen with $r = 3$ and $\theta = 0$, and the parameter τ is fixed at $\tau = 4$. The horizontal axis represents space, x, the vertical axis corresponds to time, t, and the variable $u(x,t)$ is plotted by the change in the level of color.

Therefore we have $F''(0) = 0$, $k_0 = 1$, $\hat{J}(0) = -0.2$, $\hat{J}(k_0) = 1.25$, $\hat{J}(2k_0) = 1$, and $\alpha^* = 1$, $g^* = 0.25$. The coefficients in the normal form are $A = -0.1406$, $C = D = -0.7031$, and then $M = -2.1094$, $D/M = \frac{1}{3}$. From Theorem 5.3 we obtain $L_0 : \alpha = \frac{4}{5}(g+1)$, $H_0 : [\alpha = 1,\ g > 0.25]$, $L_M : [\alpha = \frac{12}{11}(g + \frac{2}{3}),\ g > 0.25]$, $SL_S : [\alpha = \frac{6}{5}(g + \frac{7}{12}),\ g > 0.25]$, $SN_{S2} : [\alpha = \frac{444}{355}(g + \frac{61}{111}),\ g > 0.25]$, $L_m : [\alpha = 4g,\ g > 0.25]$.

We choose parameters in different regions.

Along the bifurcation line L_0 we take $\alpha = 0.95$, $g = 0.2$ in region (1) and obtain the trivial solution T, and take $\alpha = 0.98$, $g = 0.2$ in region (2) and obtain the SS pattern (Figure 14). The same set of initial conditions, say Ic1, is considered in both cases. This set of initial conditions will be used later for other parameter values.

Along the bifurcation line H_0 let us take $\alpha = 0.98$, $g = 0.26$ in region (1) (Figure 15), and $\alpha = 1.004$, $g = 0.26$ in region (7). We consider two distinct sets of initial conditions, Ic1, the same as above, and Ic2. By crossing H_0 the patterns that bifurcate from T are different: TW for Ic1 (Figure 16), and SW for Ic2, but this is unstable (see Figures 17 and 18).

Along the bifurcation line L_m we consider $\alpha = 1.08$, $g = 0.26$ in region (2) with different initial conditions Ic1 and Ic2. An SS pattern is selected (Figure 19). At $\alpha = 1.03$, $g = 0.26$ in region (3) we obtain a TW pattern for Ic1, and an SS pattern for Ic2 (Figure 20). The SS pattern is unstable, as we see when we introduce in the system white noise scaled by a factor $nz = 0.001$ (Figure 21).

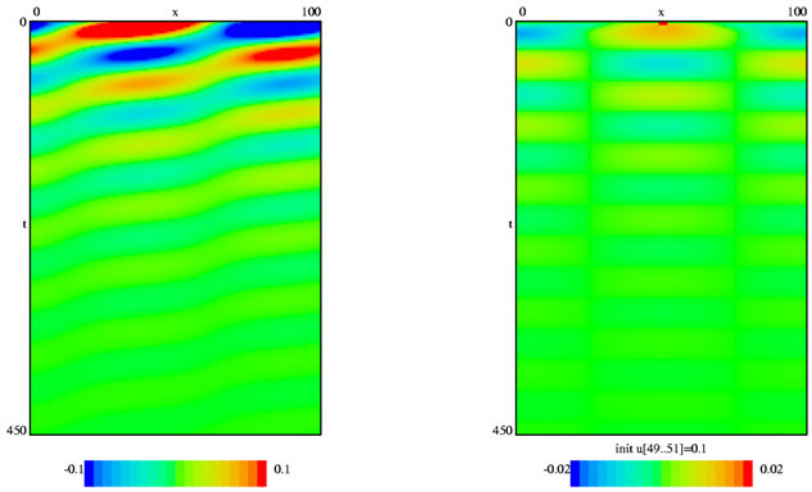

Figure 15. *At $\alpha = 0.98$, $g = 0.26$ in region* (1)*, close to the bifurcation line H_0, we obtain T for different sets of initial conditions.* (a) *Ic*1 *will give rise in region* (7) *to a TW.* (b) *Ic*2 *will give rise in region* (7) *to an unstable SW.*

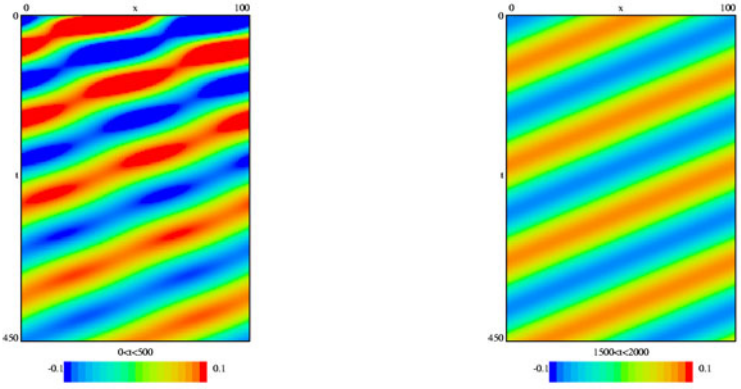

Figure 16. *The TW pattern obtained for Ic*1*, at $\alpha = 1.004$, $g = 0.26$ in region* (7)*.*

We consider $\alpha = 1.0122$, $g = 0.26$ in region (4), between SN_{S2} and SL_S, and $\alpha = 1.01122$, $g = 0.26$ in region (5), between SL_S and L_M. For different initial conditions Ic1, Ic2, and Ic3, patterns such as TW, SW, and SS, respectively, can occur, but the last two are destabilized in time to a TW. We present, for example, the numerical results for $\alpha = 1.0122$, $g = 0.26$. Starting with initial condition Ic1 we obtain a TW pattern (Figure 22); starting with Ic2, an SW pattern is formed, but it destabilizes in time to a TW (Figure 23); starting with Ic3, an SS pattern is formed, but it destabilizes in time to a TW (Figure 24).

Similar pictures are obtained for $\alpha = 1.01122$, $g = 0.26$ in region (5).

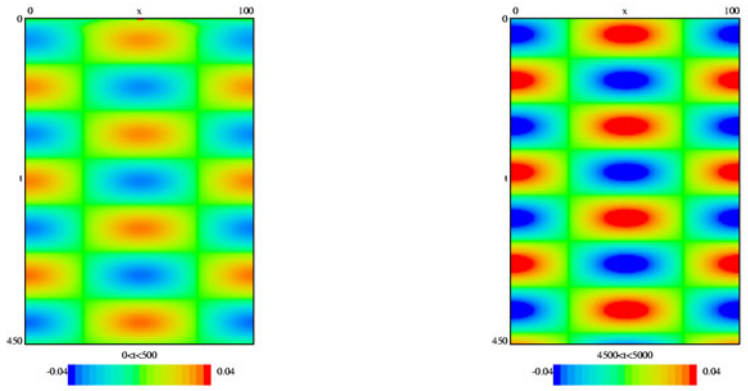

Figure 17. *The SW pattern obtained for Ic2, at $\alpha = 1.004$, $g = 0.26$ in region (7). This pattern is unstable.*

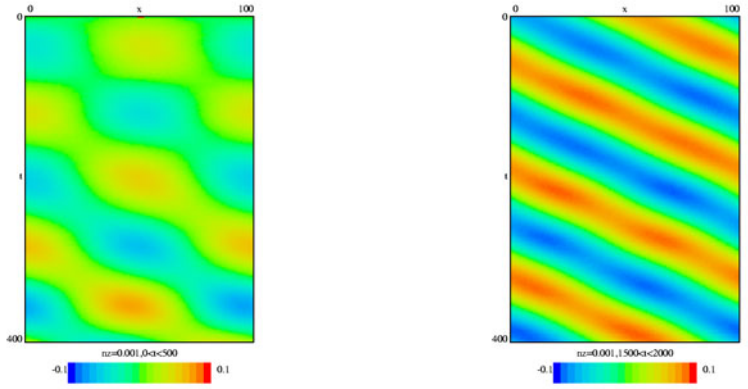

Figure 18. *The SW pattern obtained at $\alpha = 1.004$, $g = 0.26$ for Ic2 is destabilized to TW in the presence of noise.*

At $\alpha = 1.009$, $g = 0.26$ in region (6) the patterns that might occur are TW and SW, but always SW is destabilized in time to a TW (Figure 25).

Remark 12. There is a nice agreement between the theoretical and numerical results. Numerically it is impossible to detect a pattern that has all the corresponding eigenvalues positive, i.e., it is completely unstable (as one of the SWs in regions (4) and (5) in the bifurcation diagram, or the SS in region (6)). Nevertheless the other patterns that present stability at least in one direction can be visualized in the numerical simulation. Of course, eventually they will approach the only stable solution, i.e., TW.

Remark 13. We did not complete the analysis of system (1.3). A direction for future research is to investigate other possible cases (bifurcation diagrams) that might occur for different values of the parameter θ in the function F. We are especially interested in the case when the SW pattern is stable, and furthermore in the case that can give rise to an additional pattern not studied here, the MW pattern. These situations correspond to different kinds of

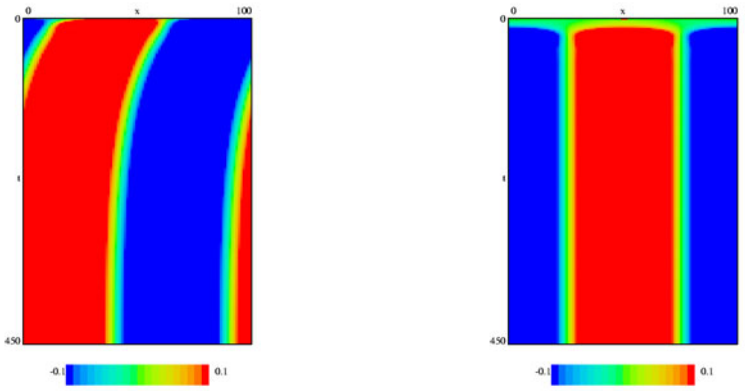

Figure 19. *The SS pattern obtained at* $\alpha = 1.08$, $g = 0.26$ *in region* (2), *close to the bifurcation line* L_m *for initial conditions* (a) $Ic1$ *and* (b) $Ic2$.

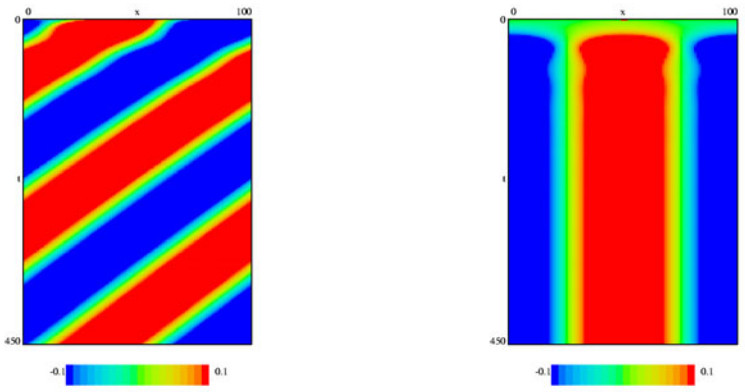

Figure 20. *At* $\alpha = 1.03$, $g = 0.26$ *in region* (3) *we obtain* (a) *TW for* $Ic1$ *and* (b) *SS for* $Ic2$ *(this pattern is unstable).*

bifurcation diagrams listed in [6]. Nevertheless, we have seen how to effect the transition from stationary patterns to TWs by varying the degree of adaptation.

6. Conclusions. We have analyzed a rate model with nonlinear sigma-shaped gain function for two homogeneous populations of neurons, one excitatory that displays adaptation, and one inhibitory. The coupling is characterized by local excitation and long range (lateral) inhibition, and the adaptation is assumed to be linear. When the strength of adaptation is sufficiently large (or the adaptation is slow enough) temporal oscillations occur in the system. In general they form TWs, but we were able to show that it is possible, when the threshold is sufficiently high, to obtain also SWs. These are spatial oscillations with frequency k_0 and temporal oscillations with frequency ω_0 that can be computed as functions of parameters τ, g, and the strength of the coupling α. Numerical simulations indicate that for a fixed adaptation time constant τ, the SW pattern occurs for an intermediate value of the strength g of

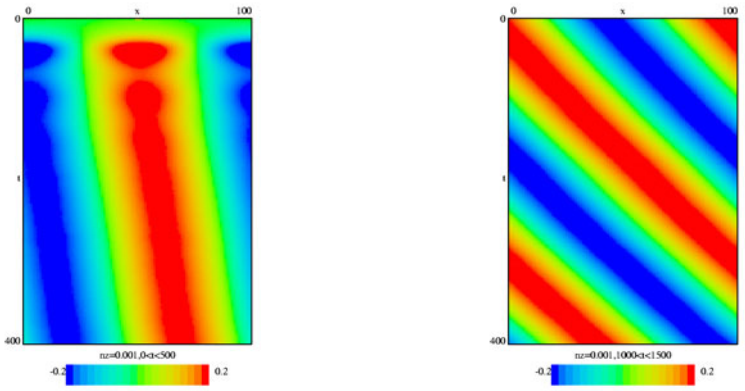

Figure 21. *The SS pattern obtained at* $\alpha = 1.03$, $g = 0.26$ *for* $Ic2$ *is destabilized to TW in the presence of noise.*

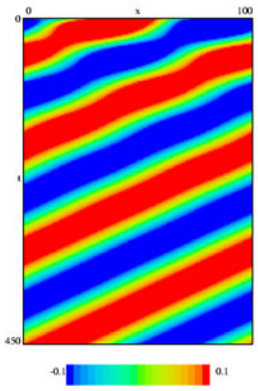

Figure 22. *At* $\alpha = 1.0122$, $g = 0.26$ *in region* (4)*, starting with* $Ic1$ *initial conditions a TW pattern is formed.*

adaptation, in a relatively small regime. When g is increased, the local activity is disrupted and starts to travel along the network, resulting in a TW pattern. Our condition for delineating the onset of stationary versus time-dependent patterns is identical to that in Hansel and Sompolinsky; they distinguish the strong and weak adaptation cases in their equations (13.80), (13.81).

We have also investigated the transition between stationary patterns and spatio-temporal patterns in the neural network, therefore explaining the patterns found in the numerical simulations of the full model. We did not complete the analysis of system (1.3). The general theory predicts, under certain conditions, the existence of a different spatio-temporal pattern, MWs characterized by two different temporal frequencies in addition to the spatial frequency k_0. The question of whether or not there are parameters regimes in the neural models in which there are MWs remains open.

We have made an assumption that there is slow negative feedback in the form of additive

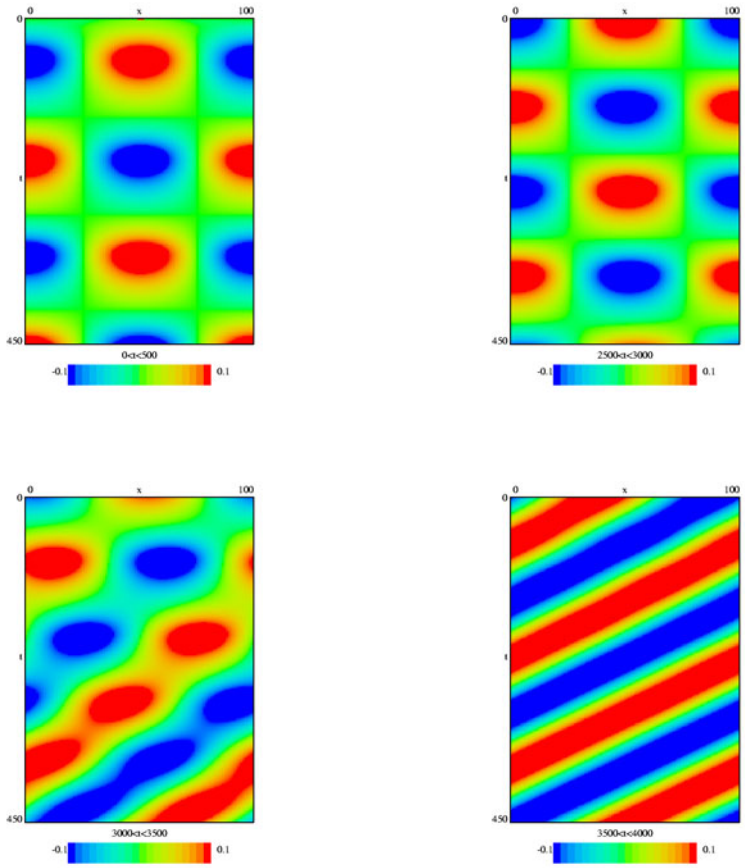

Figure 23. *At $\alpha = 1.0122$, $g = 0.26$ in region (4), starting with Ic2 initial conditions, an SW pattern is formed. Nevertheless it is destabilized in time to a TW.*

adaptation. However, this is not the only way to get slow modulation of excitation. Indeed, an alternate model could use synaptic depression. If we assume that such depression occurs for excitatory-excitatory and excitatory-inhibitory synapses, then in (1.3) we delete the $-gv$ term and replace α by αv. The v equation has the form

$$\tau \frac{dv}{dt} = q(u) - v,$$

where $q(u)$ is a monotone decreasing function of u. Thus, if u goes up, then v tends to zero corresponding to the depression of the synaptic activation. For low values of u, $q(u)$ tends to 1 so that the network is fully poised to fire. The linear stability analysis will be more complicated as will the computation of the normal forms, but we expect little change in the qualitative behavior. Other slow negative feedback mechanisms such as accumulation of intracellular sodium (leading to a reduction in the excitability) could also be modeled and would result in qualitatively similar behavior and the same basic bifurcation picture.

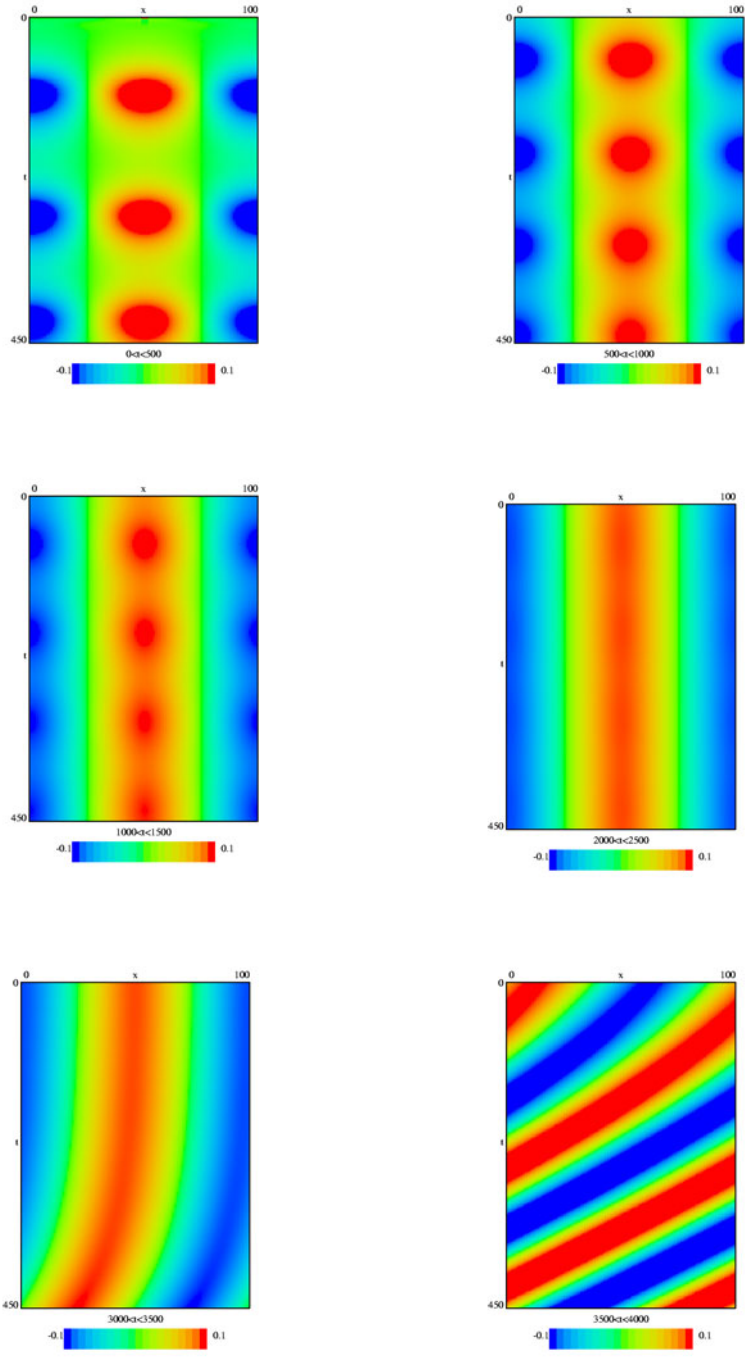

Figure 24. *At $\alpha = 1.0122$, $g = 0.26$ in region (4), starting with Ic3 initial conditions, an SS pattern is formed. Nevertheless it is destabilized in time to a TW.*

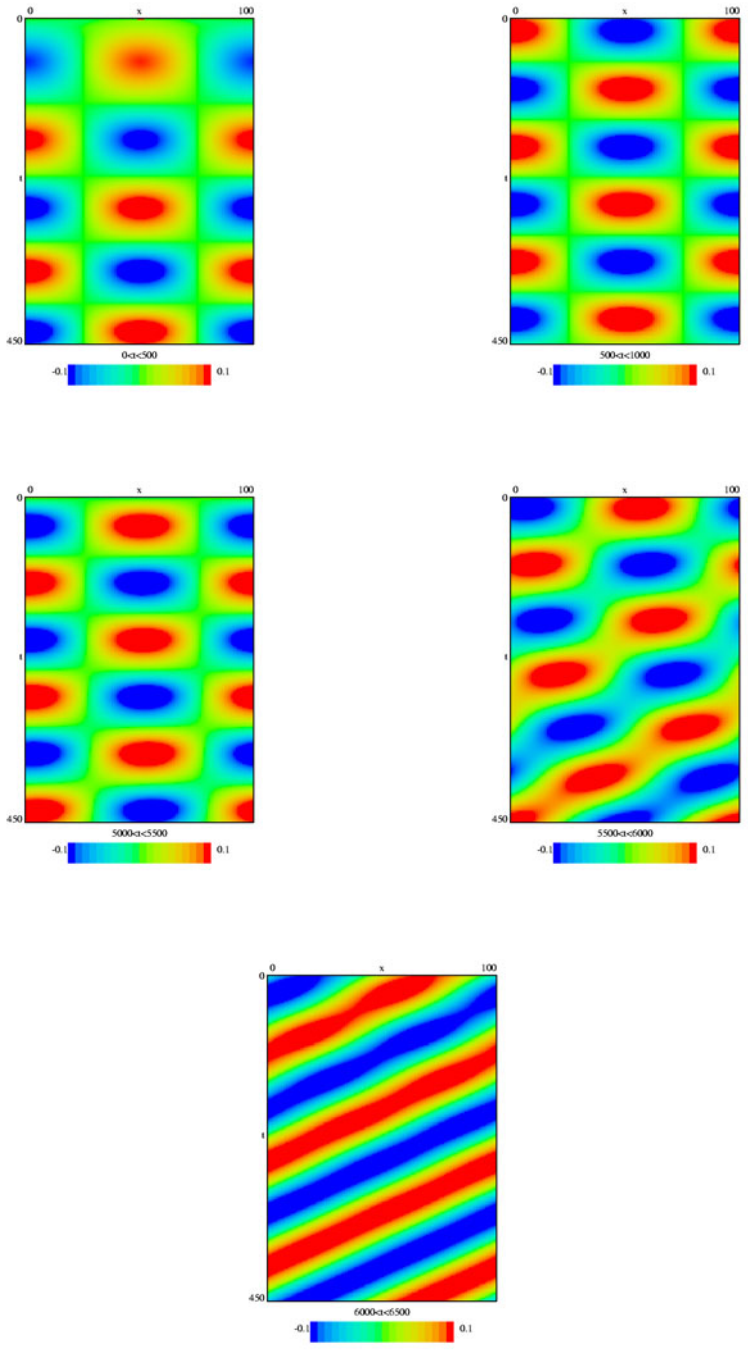

Figure 25. *At $\alpha = 1.009$, $g = 0.26$ in region (6), an SW pattern may form, but it destabilizes in time to a TW.*

We close with some speculations on the possible functional implications of the coalescence of the Hopf bifurcation and the SS bifurcation (that is, the Takens–Bogdanov bifurcation). We first point out that the original motivation of the HS model was to explain nonlinear amplification of orientation tuning. Assume that the domain is the circle so that a point x represents a specific orientation. Suppose that the time constant τ of the adaptation is small so that adaptation works quickly. Then, as we saw above, the only bifurcation is to stationary spatial patterns. As in section 3.3, let $k = 1$ be the critical wavenumber. This means that there will be a local peak at a point x_m; weak inputs will move that peak [8] so that it is pinned at a specific orientation. Thus, the network amplifies weak inputs to produce a large nonlinear response to a specific orientation. This is the *normal* state of the network. In various pathological situations, however, the network can be damaged so that this behavior is disrupted. In a recent paper, Prole, Lima, and Marrion showed that acidosis (increased pH) that occurs during epilepsy or stroke increased the time constant of both activation and inactivation of the slow voltage-dependent potassium current K_m [21]. This current is one of several that are responsible for frequency *adaptation* in cortical neurons. In the context of our simple model, this is equivalent to increasing τ_A, the time constant of adaptation. As we have shown, increasing τ_A leads to a transition from the zero eigenvalue stationary-state case to the oscillatory Hopf case. Waves have been associated with epileptic behavior in previous models (see, e.g., [20]).

The present model is for either a ring or a line of one-dimensional cortex. The actual cortex is better represented as a sheet. In this case, the dimensions of the null-space of the resulting linearized system can be much larger than studied here. For example, in the stationary pattern case, there can be stripe patterns and square patterns which bifurcate from rest. The selection between these patterns depends on the nonlinear terms in much the same way as the selection between SWs and TWs in the present paper. Two-dimensional models of cortical networks were used to explain the patterns observed during visual hallucinations [12]. Recently Bressloff and his collaborators [1] have extended the two-dimensional models to incorporate spatial connectivity and orientation selectivity in these models. Bifurcation methods should remain an important technique for the analysis of patterns in increasingly more realistic neural models.

Appendix A.

Hopf bifurcation and pattern formation. In the case of a pair of purely imaginary eigenvalues, system (2.1) can be written in the equivalent form

$$L_0 U = (\alpha - \alpha^*)\,(J * u\,,\,0)^T + B(U,U) + C(U,U,U) + \cdots \tag{A.1}$$

with

$$B(U,U) = \left(\frac{F''(0)}{2}(\alpha J * u - gv)^2, 0\right)^T,\ C(U,U,U) = \left(\frac{F'''(0)}{6}(\alpha J * u - gv)^3, 0\right)^T.$$

A good scaling for the bifurcation parameter α and the solution U we are seeking is $\alpha - \alpha^* = \epsilon^2\,\gamma$, $\gamma \in \mathbb{R}$, and

$$
\begin{aligned}
U(x,t) &= \epsilon\, U_0(x,t) + \epsilon^2\, U_1(x,t) + \epsilon^3\, U_2(x,t) + \cdots \\
&= \epsilon \begin{pmatrix} u_0 \\ v_0 \end{pmatrix} + \epsilon^2 \begin{pmatrix} u_1 \\ v_1 \end{pmatrix} + \epsilon^3 \begin{pmatrix} u_2 \\ v_2 \end{pmatrix} + \cdots .
\end{aligned} \tag{A.2}
$$

With the notation $\boldsymbol{E} = (1,0)^T$, (A.1) and (A.2) imply

(A.3)

$$
\begin{aligned}
&\epsilon L_0 U_0 + \epsilon^2 L_0 U_1 + \epsilon^3 L_0 U_2 + \mathcal{O}(\epsilon^4) = \epsilon^2 \boldsymbol{E}\, \frac{F''(0)}{2} [\alpha^* J * u_0 - g v_0]^2 \\
&+ \epsilon^3 \boldsymbol{E} \left[\gamma\, (J * u_0) + F''(0) [\alpha^* J * u_0 - g v_0][\alpha^* J * u_1 - g v_1] + \frac{F'''(0)}{6} [\alpha^* J * u_0 - g v_0]^3 \right] + \mathcal{O}(\epsilon^4);
\end{aligned}
$$

therefore the first equation to be solved is $L_0 U_0 = \mathbf{0}$.

The nullspace of L_0 corresponding to the center manifold is four-dimensional with the basis $\left\{ \Phi_0\, e^{i(\omega_0 t \pm k_0 x)}, \overline{\Phi}_0\, e^{-i(\omega_0 t \pm k_0 x)} \right\}$, and U_0 can be written as

$$
U_0 = z_1\, \Phi_0\, e^{i(\omega_0 t + k_0 x)} + w_1\, \Phi_0\, e^{i(\omega_0 t - k_0 x)} + \overline{z}_1\, \overline{\Phi}_0\, e^{-i(\omega_0 t + k_0 x)} + \overline{w}_1\, \overline{\Phi}_0\, e^{-i(\omega_0 t - k_0 x)} .
$$

Since in (A.3), $L_0 U_0 = \mathcal{O}(\epsilon)$, z_1 and w_1 are ϵ-dependent and we can write them as $z_1 = z_1(T)$ and $w_1 = w_1(T)$ with $T = \epsilon^2 t$ a slow time. These imply the singular perturbation expansions

$$
\begin{aligned}
z_1(T) &= z_1(T)_{|\epsilon=0} + z_1'(T)_{|\epsilon=0}\, \epsilon^2 t + \frac{1}{2} z_1''(T)_{|\epsilon=0}\, (\epsilon^2 t)^2 + \cdots , \\
w_1(T) &= w_1(T)_{|\epsilon=0} + w_1'(T)_{|\epsilon=0}\, \epsilon^2 t + \frac{1}{2} w_1''(T)_{|\epsilon=0}\, (\epsilon^2 t)^2 + \cdots .
\end{aligned}
$$

For simplicity we introduce the notation $z_2 = z_1(T)_{|\epsilon=0}$, $\dot{z}_2 = z_1'(T)_{|\epsilon=0}$, $w_2 = w_1(T)_{|\epsilon=0}$, $\dot{w}_2 = w_1'(T)_{|\epsilon=0}$. The dot shows the derivation of z_2 and w_2 with respect to the slow time T.

We obtain then $z_1 = z_2 + \dot{z}_2\, \epsilon^2 t + \mathcal{O}(\epsilon^4)$, $w_1 = w_2 + \dot{w}_2\, \epsilon^2 t + \mathcal{O}(\epsilon^4)$, and

$$
\begin{aligned}
U_0 = \Big[& z_2\, \Phi_0\, e^{i(\omega_0 t + k_0 x)} + w_2\, \Phi_0\, e^{i(\omega_0 t - k_0 x)} \\
& + \overline{z}_2\, \overline{\Phi}_0\, e^{-i(\omega_0 t + k_0 x)} + \overline{w}_2\, \overline{\Phi}_0\, e^{-i(\omega_0 t - k_0 x)} \Big] + \mathcal{O}(\epsilon^2) .
\end{aligned}
$$

Remark 14. The calculation of the normal form is cumbersome (see [5] for details of proofs). The normal form results by solving for U_1 and U_2 in the corresponding functional equations implied by (A.3), and it is

$$
\begin{cases}
\dot{z}_2 = z_2\, (\, \tilde{a} + b\, z_2\, \overline{z}_2 + c\, w_2\, \overline{w}_2\,) , \\
\dot{w}_2 = w_2\, (\, \tilde{a} + b\, w_2\, \overline{w}_2 + c\, z_2\, \overline{z}_2\,) ,
\end{cases} \tag{A.4}
$$

with $\tilde{a} = a/\epsilon^2$, $a = \hat{J}(k_0)(\alpha - \alpha^*)\left(\frac{1}{2} - i \frac{1}{2\sqrt{g\tau - 1}}\right)$, and b, c constants [5]. We notice that, as a result of the scaling $z(t) = \epsilon\, z_2(T)$, $w(t) = \epsilon\, w_2(T)$ with $T = \epsilon^2 t$ (therefore $z' = dz/dt = \epsilon^3 \dot{z}_2$

and $w' = dw/dt = \epsilon^3 \dot{w}_2$), system (A.4) takes exactly the form (3.5) and, indeed, the linear approximation of $U(x,t)$ is (3.4).

Normal form for the pitchfork bifurcation. We fix the values of τ and g such that $g < 1/\tau$ and take α as the bifurcation parameter. The bifurcation value around which we will consider the singular perturbation analysis is α^* from (4.1), and, in the following, the operator L_0 and the matrix $\hat{L}(k)$ are evaluated at $\alpha = \alpha^*$.

The singular perturbation expansion for the parameter α and solution $U(x,t)$ follows exactly the same steps as in (A.1), (A.2), and (A.3). The nullspace of L_0 corresponding to the center manifold is now only two-dimensional and has the basis $\{\Phi_0\, e^{\pm ik_0 x}\}$, so U_0 can be written as

$$U_0 = z_1\, \Phi_0\, e^{ik_0 x} + \overline{z}_1\, \Phi_0\, e^{-ik_0 x}$$

with z_1 depending on the slow time $T = \epsilon^2 t$, that is, $z_1 = z_1(T)$.

As in the previous subsection, we can write the singular perturbation expansion of z_1 as $z_1 = z_2 + \dot{z}_2\, \epsilon^2 t + \mathcal{O}(\epsilon^4)$. Then the equation that defines U_1 becomes

$$L_0 U_1 = \frac{F''(0)}{2} \boldsymbol{E} \left[z_2^2\, e^{2ik_0 x} + \overline{z}_2^2\, e^{-2ik_0 x} + 2 z_2\, \overline{z}_2 \right].$$

Therefore U_1 takes the form

$$\begin{aligned} U_1 &= \xi_1\, z_1^2\, e^{2ik_0 x} + \xi_1\, \overline{z}_1^2\, e^{-2ik_0 x} + 2\xi_2\, z_1\, \overline{z}_1 \\ &= \xi_1\, z_2^2\, e^{2ik_0 x} + \xi_1\, \overline{z}_2^2\, e^{-2ik_0 x} + 2\xi_2\, z_2\, \overline{z}_2 + \mathcal{O}(\epsilon^2) \end{aligned}$$

with ξ_1, ξ_2 defined by $\left[-\hat{L}(2k_0)\xi_1\right] = \frac{F''(0)}{2}\boldsymbol{E}$, $\left[-\hat{L}(0)\xi_2\right] = \frac{F''(0)}{2}\boldsymbol{E}$. The normal form corresponding to a zero eigenvalue results by solving the functional equation for U_2, and it is

$$\dot{z}_2 = z_2(\, \tilde{\eta}_1 + \Lambda z_2\, \overline{z}_2\,) \tag{A.5}$$

with $\tilde{\eta}_1 = \eta_1/\epsilon^2$, $\eta_1 = \frac{\hat{J}(k_0)(\alpha - \alpha^*)}{1 - g\tau}$, and Λ defined by (4.3).

We notice that $U = \epsilon U_0 + \mathcal{O}(\epsilon^2) = \epsilon\, z_2\, \Phi_0\, e^{ik_0 x} + \epsilon\, \overline{z}_2\, \Phi_0\, e^{-ik_0 x} + \mathcal{O}(\epsilon^2)$. With the choice of $z(t) = \epsilon\, z_2(T)$, $T = \epsilon^2 t$, (A.5) is equivalent to

$$z' = \frac{\hat{J}(k_0)}{1 - g\tau}(\alpha - \alpha^*) z + \Lambda |z|^2 z\,,$$

which is the normal form at zero eigenvalue written in the original parameters.

Normal form for the double-zero bifurcation with $O(2)$-symmetry. In the case of a double-zero eigenvalue, we choose the singular perturbation expansion for α, g and the solution U as $\alpha - \alpha^* = \epsilon^2\, \gamma$, $g - g^* = \epsilon^2\, \eta$, $\gamma, \eta \in \mathbb{R}$,

$$U(x,t) = \epsilon\, U_0(x,t) + \epsilon^2\, U_1(x,t) + \epsilon^3\, U_2(x,t) + \epsilon^4\, U_3(x,t) + \cdots\,. \tag{A.6}$$

The system equivalent to (2.1) is then

$$L_0U = (\alpha-\alpha^*)\,L_1U + (g-g^*)\,L_2U + B(U,U) + C(U,U,U) + Q(U,U,U,U) + \cdots, \tag{A.7}$$

where $B(U,U)$, $C(U,U,U)$, $Q(U,U,U,U)$ represent the quadratic, cubic, and fourth order terms, L_0 is defined according to Remark 10, and

$$L_1 = \begin{pmatrix} J*(\cdot) & 0 \\ 0 & 0 \end{pmatrix}, \quad L_2 = \begin{pmatrix} 0 & -1 \\ 0 & 0 \end{pmatrix}.$$

With the notation $\boldsymbol{E}$ for the unit vector $(1,0)^T$, (A.7) becomes

$$\begin{aligned}
&\epsilon L_0U_0 + \epsilon^2\left[L_0U_1 - \frac{F''(0)}{2}[\alpha^*\,J*u_0 - g^*v_0]^2\boldsymbol{E}\right] + \epsilon^3[\,L_0U_2 - \gamma\,L_1U_0 - \eta\,L_2U_0\,] \\
&\qquad + \epsilon^4[\,L_0U_3 - \gamma\,L_1U_1 - \eta\,L_2U_1\,] \\
&= \epsilon^3\left[F''(0)[\alpha^*\,J*u_0 - g^*v_0][\alpha^*\,J*u_1 - g^*v_1] + \frac{F'''(0)}{6}[\alpha^*\,J*u_0 - gv_0]^3\right]\boldsymbol{E} \\
&\qquad + \epsilon^4\left[\frac{F''(0)}{2}[\alpha^*\,J*u_1 - g^*v_1]^2 + F''(0)[\alpha^*\,J*u_0 - g^*v_0][\alpha^*\,J*u_2 - g^*v_2\right. \\
&\qquad\qquad + \gamma\,J*u_0 - \eta\,v_0] + \frac{F'''(0)}{2}[\alpha^*\,J*u_0 - gv_0]^2[\alpha^*\,J*u_1 - gv_1] \\
&\qquad\qquad \left. + \frac{F^{(4)}(0)}{24}[\alpha^*\,J*u_0 - gv_0]^4\right]\boldsymbol{E} + \mathcal{O}(\epsilon^5)\,.
\end{aligned} \tag{A.8}$$

In order to construct the normal form we need to identify the functional equations that U_0, U_1, U_2, and U_3 satisfy and then solve for them [5].

The nullspace of L_0 corresponding to the center manifold is now only two-dimensional with the basis $\left\{\Phi_0\,e^{\pm ik_0x}\right\}$, where Φ_0 is the real vector defined in (5.2). As a consequence, U_0 can be written as

$$U_0 = \left(z_1\,e^{ik_0x} + \overline{z}_1\,e^{-ik_0x}\right)\Phi_0$$

with $z_1 = z_1(T)$, where $T = \epsilon t$ is the appropriate slow time. Then

$$z_1(T) = z_1(T)_{|\epsilon=0} + z_1'(T)_{|\epsilon=0}\,\epsilon t + \frac{1}{2}z_1''(T)_{|\epsilon=0}\,(\epsilon t)^2 + \frac{1}{6}z_1'''(T)_{|\epsilon=0}\,(\epsilon t)^3 + \mathcal{O}(\epsilon^4)$$

or, with notation $z_2 = z_1(T)_{|\epsilon=0}$, $\dot{z}_2 = z_1'(T)_{|\epsilon=0}$,

$$z_1 = z_2 + \dot{z}_2\,\epsilon t + \frac{1}{2}\,\ddot{z}_2\,(\epsilon t)^2 + \frac{1}{6}\dddot{z}_2\,(\epsilon t)^3 + \mathcal{O}(\epsilon^4)\,.$$

Therefore $U_0 = \left(z_2\,e^{ik_0x} + \overline{z}_2\,e^{-ik_0x}\right)\Phi_0 + \mathcal{O}(\epsilon)$.

The equation that defines U_1 reads as

$$L_0U_1 = -\left[\dot{z}_2\,e^{ik_0x} + \dot{\overline{z}}_2\,e^{-ik_0x}\right]\,\Phi_0 + \frac{F''(0)}{2\tau}\boldsymbol{E}\left[z_2^2\,e^{2ik_0x} + \overline{z}_2^2\,e^{-2ik_0x} + 2z_2\,\overline{z}_2\right]$$

and U_1 can be constructed as

$$U_1 = \left[w_1\, e^{ik_0x} + \overline{w}_1\, e^{-ik_0x}\right] \Phi_1 + z_1^2\xi_1\, e^{2ik_0x} + \overline{z}_1^2\xi_1\, e^{-2ik_0x} + 2z_1\,\overline{z}_1\xi_2$$

with ξ_1, ξ_2 real vectors and $w_1 = w_1(T)$, or, similar to the singular perturbation expansion of z_1,

$$w_1 = w_2 + \dot{w}_2\,\epsilon t + \frac{1}{2}\ddot{w}_2\,\epsilon^2 t^2 + \mathcal{O}(\epsilon^3)\,.$$

The first equation of the normal form is obtained by solving for U_1 and it is $\dot{z}_2 = w_2$. The next two steps consist of finding U_2 as

$$U_2 = \left[z_1 w_1 e^{2ik_0x} + \overline{z}_1\,\overline{w}_1 e^{-2ik_0x}\right]\beta_1 + [z_1\,\overline{w}_1 + \overline{z}_1\,w_1]\beta_2 + \left[z_1^3 e^{3ik_0x} + \overline{z}_1^3 e^{-3ik_0x}\right]\beta_3$$

with $\beta_1, \beta_2, \beta_3$ real vectors to be computed. Then we need to solve for U_3 [5].

As a consequence we obtain the normal form

$$\text{(A.9)}\qquad \begin{cases} \dot{z}_2 = w_2\,, \\ \dot{w}_2 = \frac{\gamma\hat{J}(k_0)-\eta}{\tau} z_2 + A|z_2|^2 z_2 \\ \qquad\qquad + \epsilon\{\gamma\hat{J}(k_0)w_2 + Cz_2[\overline{z}_2 w_2 + z_2\overline{w}_2] + D|z_2|^2 w_2\} + \mathcal{O}(\epsilon^2)\,, \end{cases}$$

where $\gamma = (\alpha - \alpha^*)/\epsilon^2$ and $\eta = (g - g^*)/\epsilon^2$.

With the proper scaling $z(t) = \epsilon z_2(T)$, $w(t) = \epsilon^2 w_2(T)$, we have $z' = \epsilon^2\dot{z}_2$, $w' = \epsilon^3\dot{w}_2$, and (A.9) is equivalent to the normal form (5.5).

Remark 15. If we consider the solution U of the nonlinear system approximated only by its projection on the generalized eigenspace, we have

$$\begin{aligned} U(x,t) &\approx 2\epsilon\,\Phi_0\,\mathrm{Re}\left[z_2(T)\,e^{ik_0x}\right] + 2\epsilon^2\,\Phi_1\,\mathrm{Re}\left[w_2(T)\,e^{ik_0x}\right] \\ &\approx 2\,\Phi_0\,\mathrm{Re}\left[z(t)\,e^{ik_0x}\right] + 2\,\Phi_1\,\mathrm{Re}\left[w(t)\,e^{ik_0x}\right] \end{aligned}$$

and this is exactly the formula (5.4).

Appendix B. Additional material. The transitions from an unstable to a new stable pattern as a parameter is changed are shown in the following files. In each case, a pattern that was stable for one set of parameters is used as an initial condition for the new parameter. Often the patterns go through several intermediate transient states before settling into a final stable state. The main parameter that is varied is the threshold since this has no effect on the linear stability but rather affects the selection between patterns.

Animation 1. The initial data and parameter values are as in Figure 4. We start with $\theta = 0.3$ and initial conditions close to a TW which is stable for $\theta = 0.0$. The pattern evolves and stabilizes to an SW.

Animation 2. The last conditions in Animation 1 are chosen as initial conditions in Animation 2 and the value of parameter θ is changed to $\theta = 0$. The resulting stable pattern is now a TW.

Animation 4. This pattern is taken from the results of section 5.2 (Figure 24). An SW pattern is selected and then destabilized to a TW. Note the initial transition to a stationary pattern before switching to a TW.

Animation 5. The results presented in Figure 25 are shown here. An SW pattern is selected and destabilized to a TW.

Acknowledgment. Rodica Curtu thanks the University of Pittsburgh for support in the form of an Andrew Mellon Predoctoral Fellowship for her thesis work.

REFERENCES

[1] P. C. Bressloff, J. D. Cowan, M. Golubitsky, P. J. Thomas, and M. Wiener, *Geometric visual hallucinations, Euclidean symmetry and the functional architecture of striate cortex*, Philos. Trans. Roy. Soc. Lond. Ser. B, 40 (2001), pp. 299–330.

[2] R. D. Chervin, P. A. Pierce, and B. W. Connors, *Periodicity and directionality in the propagation of epileptiform discharges across neocortex*, J. Neurophysiol., 60 (1988), pp. 1695–1713.

[3] B. W. Connors and M. J. Gutnick, *Intrinsic firing patterns of diverse neocortical neurons*, Trends Neurosci., 13 (1990), pp. 99–104.

[4] B. W. Connors, M. J. Gutnick, and D. A. Prince, *Electrophysiological properties of neocortical neurons in vitro*, J. Neurophysiol., 48 (1982), pp. 1302–1320.

[5] R. Curtu, *Waves and Oscillations in Model Neuronal Networks*, Ph.D. Dissertation, Department of Mathematics, University of Pittsburgh, Pittsburgh, PA, 2003.

[6] G. Dangelmayr and E. Knobloch, *The Takens-Bogdanov bifurcation with $O(2)$-symmetry*, Philos. Trans. Roy. Soc. Lond. Ser. A, 322 (1987), pp. 243–279.

[7] B. Ermentrout, *Simulating, Analyzing, and Animating Dynamical Systems: A Guide to XPPAUT for Researchers and Students*, SIAM, Philadelphia, 2002.

[8] G. B. Ermentrout, *Neural networks as spatio-temporal pattern-forming systems*, Rep. Progr. Phys., 61 (1998), pp. 353–430.

[9] B. Ermentrout, *Stripes or spots? Nonlinear effects in bifurcation of reaction-diffusion equations on the square*, Proc. Roy. Soc. Lond. Ser. A, 434 (1991), pp. 413–417.

[10] G. B. Ermentrout, *Symmetry Breaking in Homogeneous, Isotropic, Stationary Neuronal Nets*, Ph.D. Dissertation, The University of Chicago, Chicago, IL, 1979.

[11] G. B. Ermentrout, J. Campbell, and G. Oster, *A model for shell patterns based on neural activity*, The Veliger, 28 (1986), pp. 369–388.

[12] G. B. Ermentrout and J. Cowan, *A mathematical theory of visual hallucination patterns*, Biol. Cybern., 34 (1979), pp. 137–150.

[13] G. B. Ermentrout and D. Kleinfeld, *Traveling electrical waves in cortex: Insights from phase dynamics and speculation on a computational role*, Neuron, 29 (2001), pp. 33–44.

[14] M. J. Gutnick, B. W. Connors, and D. A. Prince, *Mechanisms of neocortical epileptogenesis in vitro*, J. Neurophysiol., 48 (1982), pp. 1321–1335.

[15] D. Hansel and H. Sompolinsky, *Modeling feature selectivity in local cortical circuits*, in Methods in Neuronal Modeling: From Ions to Networks, 2nd ed., C. Koch and I. Segev, eds., MIT Press, Cambridge, MA, 1998.

[16] D. Hubel and T. Wiesel, *Receptive fields and functional architecture of monkey striate cortex*, J. Physiol., 195 (1968), pp. 215–243.

[17] E. Knobloch and J. de Luca, *Amplitude equations for travelling wave convection*, Nonlinearity, 3 (1990), pp. 975–980.

[18] C. R. Laing and C. C. Chow, *A spiking neuron model for binocular rivalry*, J. Comp. Neurosci., 12 (2002), pp. 39–53.

[19] J. D. Murray, *Mathematical Biology*, 2nd ed., Springer, New York, 1998.

[20] D. J. Pinto and G. B. Ermentrout, *Spatially structured activity in synaptically coupled neuronal networks*: I. *Traveling fronts and pulses*, SIAM J. Appl. Math., 62 (2001), pp. 206–225.

[21] D. L. Prole, P. A. Lima, and N. V. Marrion, *Mechanisms underlying modulation of neuronal KCNQ2/KCNQ3 potassium channels by extracellular protons*, J. Gen. Physiol., 122 (2003), pp. 775–793.
[22] N. V. Swindale, *A model for the formation of ocular dominance stripes*, Proc. Roy. Soc. Lond. Ser. B, 208 (1980), pp. 243–264.
[23] H. R. Wilson, *Spikes, Decisions, and Actions*, Oxford University Press, Oxford, UK, 1999.
[24] H. R. Wilson and J. D. Cowan, *A mathematical theory of the functional dynamics of cortical and thalamic nervous tissue*, Kybernetik, 13 (1973), pp. 55–80.
[25] X. Xie, R. H. R. Hahnloser, and H. S. Seung, *Double-ring network model of the head-direction system*, Phys. Rev. E, 66 (2002), 041902.